Journal of Elasticity
https://doi.org/10.1007/s10659-024-10056-x

RESEARCH

A Reformulation of the Browaeys and Chevrot Decomposition of Elastic Maps

Walter Tape[1] **· Carl Tape**[2]

Received: 15 September 2023 / Accepted: 20 February 2024

Abstract
An elastic map **T** associates stress with strain in some material. A symmetry of **T** is a rotation of the material that leaves **T** unchanged, and the symmetry group of **T** consists of all such rotations. The symmetry class of **T** describes the symmetry group but without the orientation information. With an eye toward geophysical applications, Browaeys & Chevrot developed a theory which, for any elastic map **T** and for each of six symmetry classes Σ, computes the "Σ-percentage" of **T**. The theory also finds a "hexagonal approximation"—an approximation to **T** whose symmetry class is at least transverse isotropic. We reexamine their theory and recommend that the Σ-percentages be abandoned. We also recommend that the hexagonal approximations to **T** be replaced with the closest transverse isotropic maps to **T**.

Keywords Elastic symmetry · Elasticity · Theoretical seismology · Geophysics

Mathematics Subject Classification 74B05 · 86A15 · 86-04

1 Introduction

An elastic map **T** expresses the constitutive relations or generalized Hooke's law for a material; it associates stress with strain at a point **p** in the material. A symmetry of **T** is a rotation of the material about **p** that leaves **T** unchanged, and the symmetry group of **T** consists of all such rotations. The symmetry class of **T**, intuitively, is its symmetry group but stripped of the orientation information.

For any elastic map of arbitrary symmetry, Browaeys & Chevrot [9] wanted to be able to approximate it by an elastic map having "hexagonal" symmetry. They also wanted to express the percentages—in some sense still not clear to us—of certain symmetry classes in the map. They introduced a distinctive decomposition of elastic maps that was supposed to be the basis for getting the hexagonal approximation and the percentages.

✉ C. Tape
ctape@alaska.edu

W. Tape
wtape@alaska.edu

[1] Department of Mathematics, University of Alaska, Fairbanks, AK 99775, USA

[2] Geophysical Institute and Dept. of Geosciences, University of Alaska, Fairbanks, AK 99775, USA

Published online: 08 March 2024

We have reformulated the material on decompositions, hexagonal approximation, and percentages. The exposition of Browaeys & Chevrot [9] is sparse in places, and we have sometimes had to rely more on Walker & Wookey [57–59] than on Browaeys & Chevrot [9] themselves.

Three advances since the time of the Browaeys and Chevrot paper suggest that the paper indeed deserves another look. First, we now have visualization tools that were not available earlier [19]. Second, we understand better the structure of the space of elastic maps. Third, we can now find more easily the symmetry group of any given elastic map [8, 20, 54]. (In Browaeys and Chevrot [9], the problem of finding the symmetry group was supposed to be tackled using the methods of Cowin & Mehrabadi [15].)

In the end, we recommend abandoning the percentages. We also recommend abandoning the hexagonal approximation, except in the special case where it coincides with the closest transverse isotropic map of Dellinger [18] or Diner et al. [19]. The decomposition itself turns out to be nearly irrelevant.

The elastic maps used in our examples are not meant to be physically realistic, except that all are positive definite.

A substantial number of authors have relied on Browaeys & Chevrot [9]; see our Sect. 14.

2 Orthogonal Projection

We recall the key features of orthogonal projection: In an inner product space $\mathcal{T}$, the orthogonal projection $\mathbf{P}(\mathbf{T}, \mathcal{V})$ of $\mathbf{T} \in \mathcal{T}$ onto a subspace $\mathcal{V}$ of $\mathcal{T}$ is characterized by

$$\mathbf{T}_1 = \mathbf{P}(\mathbf{T}, \mathcal{V}) \iff \begin{cases} \mathbf{T}_1 \in \mathcal{V}, & \text{(1a)} \\ \mathbf{T} - \mathbf{T}_1 \in \mathcal{V}^\perp. & \text{(1b)} \end{cases}$$

The orthogonal complement $\mathcal{V}^\perp$ of $\mathcal{V}$ consists of the members of $\mathcal{T}$ that are orthogonal to all the members of $\mathcal{V}$.

The distance from $\mathbf{T}$ to the subspace $\mathcal{V}$ is

$$d(\mathbf{T}, \mathcal{V}) = \|\mathbf{T} - \mathbf{P}(\mathbf{T}, \mathcal{V})\|. \tag{2}$$

Since $\mathbf{T} \cdot \mathbf{T}_1 = ((\mathbf{T} - \mathbf{T}_1) + \mathbf{T}_1) \cdot \mathbf{T}_1 = \|\mathbf{T}_1\|^2$, the angle between $\mathbf{T}$ and $\mathbf{T}_1$ is

$$\angle(\mathbf{T}, \mathbf{T}_1) = \cos^{-1} \frac{\mathbf{T} \cdot \mathbf{T}_1}{\|\mathbf{T}\| \|\mathbf{T}_1\|} = \cos^{-1} \frac{\|\mathbf{T}_1\|}{\|\mathbf{T}\|}. \tag{3}$$

The angle $\angle(t\mathbf{T}, \mathbf{P}(t\mathbf{T}, \mathcal{V}))$ is independent of $t \in \mathbb{R}$, $t \neq 0$, since the projection function $\mathbf{T} \to \mathbf{P}(\mathbf{T}, \mathcal{V})$ is linear.

For subspaces $\mathcal{V}_1$ and $\mathcal{V}_2$ of $\mathcal{T}$, it follows from Eqs. (1a) and (1b) that

$$\mathcal{V}_1 \subset \mathcal{V}_2 \implies \mathbf{P}\Big(\mathbf{P}(\mathbf{T}, \mathcal{V}_2), \mathcal{V}_1\Big) = \mathbf{P}(\mathbf{T}, \mathcal{V}_1). \tag{4}$$

3 The Elastic Symmetry Groups

Let $\mathbb{U}$ be the group of all 3×3 rotation matrices, and let $V \in \mathbb{U}$. If an elastic map $\mathbf{T}$ describes the elasticity in a certain material at a point $\mathbf{p}$, then $\overline{V} \circ \mathbf{T} \circ \overline{V}^*$ does the same after the

Table 1 Notation pertaining to elastic maps

$\mathbb{M}$	Inner product space of all 3×3 symmetric matrices (strains or stresses).
$\mathbf{T} : \mathbb{M} \to \mathbb{M}$	An elastic map, that is, a self-adjoint linear transformation from $\mathbb{M}$ to $\mathbb{M}$.
$\boldsymbol{\mathcal{T}}$	Inner product space of all elastic maps.
Σ	One of the labels ISO, XISO, TET, ORTH, MONO, TRIV, CUBE, TRIG.
$\Sigma_{\mathbf{T}}$	Symmetry class of $\mathbf{T}$.
$\mathbb{U}$	Group of all 3×3 rotation matrices.
$\mathcal{S}_{\mathbf{T}} \subset \mathbb{U}$	Symmetry group of $\mathbf{T}$, consisting of all symmetries of $\mathbf{T}$.
$\mathbb{U}_\Sigma \subset \mathbb{U}$	Reference group (Table 2).
$\mathbb{Z}_2(\mathcal{S}_{\mathbf{T}})$	Set of 2-fold points of $\mathcal{S}_{\mathbf{T}}$.
$\boldsymbol{\mathcal{T}}_\Sigma \subset \boldsymbol{\mathcal{T}}$	Set of elastic maps having symmetry at least Σ. Equation (14).
$\boldsymbol{\mathcal{V}}_\Sigma(U) \subset \boldsymbol{\mathcal{T}}_\Sigma$	Eq. (15).
$\mathbf{P}(\mathbf{T}, \boldsymbol{\mathcal{V}}_\Sigma(U))$	Orthogonal projection of the elastic map $\mathbf{T}$ to the subspace $\boldsymbol{\mathcal{V}}_\Sigma(U)$.
$\mathbf{X}(\mathbf{T}, U)$	XISO-approximation to $\mathbf{T}$ determined by U. Equation (43).
$\mathbf{A}(\mathbf{T}, U)$	Eq. (24b).
$\overline{U} : \mathbb{M} \to \mathbb{M}$	Conjugation by $U \in \mathbb{U}$. That is, $\overline{U}(E) = UEU^\top$, $E \in \mathbb{M}$.
$\overline{U}^*$	Adjoint of $\overline{U}$. It is conjugation by $U^\top$.
$d(\mathbf{T}_1, \mathbf{T}_2)$	Distance between elastic maps $\mathbf{T}_1$ and $\mathbf{T}_2$.
$d(\mathbf{T}, \boldsymbol{\mathcal{T}}')$	Distance between $\mathbf{T}$ and a subset $\boldsymbol{\mathcal{T}}'$ of $\boldsymbol{\mathcal{T}}$.
$\mathbb{B}$	The basis for $\mathbb{M}$ in Eq. (80).
$[\mathbf{T}]_{\mathbb{B}\mathbb{B}}$	Matrix representation of $\mathbf{T}$ with respect to $\mathbb{B}$.

material has been rotated about $\mathbf{p}$ by V. (See Table 1 for $\overline{V}$ and $\overline{V}^*$. The symbol "$\circ$" denotes composition of functions.) Thus V is said to be a symmetry of $\mathbf{T}$ if

$$\overline{V} \circ \mathbf{T} \circ \overline{V}^* = \mathbf{T}. \tag{5}$$

All such V make up the symmetry group $\mathcal{S}_{\mathbf{T}}$ of $\mathbf{T}$. For $U \in \mathbb{U}$ we find from Eq. (5) that

$$\mathcal{S}_{\overline{U} \circ \mathbf{T} \circ \overline{U}^*} = U \mathcal{S}_{\mathbf{T}} U^\top. \tag{6}$$

A subgroup $\mathbb{V}$ of $\mathbb{U}$ is an elastic symmetry group if $\mathbb{V} = \mathcal{S}_{\mathbf{T}}$ for some elastic map $\mathbf{T}$. The eight reference groups $\mathbb{U}_\Sigma$ in Table 2 are elastic symmetry groups, as are their conjugates $U\mathbb{U}_\Sigma U^\top$. Conversely, as shown by Forte and Vianello [24], if $\mathbb{V}$ is an elastic symmetry group, then

$$\mathbb{V} = U\mathbb{U}_\Sigma U^\top \tag{7}$$

for some $U \in \mathbb{U}$ and for one of the reference groups $\mathbb{U}_\Sigma$.

For any group of rotation matrices, its 2-fold points are the points where the axes of its 2-fold rotations intersect the unit sphere $\mathbb{S}^2$. The 2-fold points of $\mathbb{U}_{\text{MONO}}$, for example, are the north and south poles of $\mathbb{S}^2$. The 2-fold points of $\mathbb{U}_{\text{XISO}}$ are the north and south poles together with all points on the equator. For any group $\mathbb{W} \subset \mathbb{U}$ we let $\mathbb{Z}_2(\mathbb{W})$ denote the set of its 2-fold points. Then

$$\mathbb{Z}_2(V\mathbb{W}V^\top) = V(\mathbb{Z}_2(\mathbb{W})) \qquad (V \in \mathbb{U}). \tag{8}$$

Table 2 The eight reference groups $\mathbb{U}_\Sigma$ for elastic symmetry. The first six groups are those appearing along the red path in Fig. 2a. Each of the six contains the group below it as a subgroup. The matrices in $\mathbb{U}_{\text{XISO}}$ are the rotations about the z-axis together with the 2-fold rotations about axes in the xy-plane. The matrix I is the 3×3 identity matrix. The matrices X_ξ, Y_ξ, Z_ξ are the rotations through angle ξ about the x, y, z-axes, respectively. The matrix $1\ \bar{1}\ 0_2$ is the 2-fold rotation about the axis $(1, -1, 0)$, and $0\ 0\ 1_4$ is the 4-fold rotation about $(0, 0, 1)$. ISO = isotropic, XISO = transverse isotropic, TET = tetragonal, ORTH = orthorhombic, MONO = monoclinic, TRIV = trivial, CUBE = cubic, TRIG = trigonal.

Group	Members
$\mathbb{U}_{\text{ISO}} = \mathbb{U}$	All rotations
$\mathbb{U}_{\text{XISO}}$	All rotations U such that $U\mathbf{k} = \pm\mathbf{k}$ $(\mathbf{k} = (0, 0, 1))$
$\mathbb{U}_{\text{TET}}$	I, X_π, Y_π, Z_π, $1\ 1\ 0_2$, $1\ \bar{1}\ 0_2$, $0\ 0\ 1_4$, $0\ 0\ \bar{1}_4$
$\mathbb{U}_{\text{ORTH}}$	I, X_π, Y_π, Z_π
$\mathbb{U}_{\text{MONO}}$	I, Z_π
$\mathbb{U}_{\text{TRIV}}$	I
$\mathbb{U}_{\text{CUBE}}$	The 24 rotational symmetries of the cube with vertices $(\pm 1, \pm 1, \pm 1)$
$\mathbb{U}_{\text{TRIG}}$	I, $\sqrt{3}\ 1\ 0_2$, Y_π, $\sqrt{3}\ \bar{1}\ 0_2$, $0\ 0\ 1_3$, $0\ 0\ \bar{1}_3$

From Table 2 and Eq. (7), each elastic symmetry group is generated by its own 2-fold rotations. Hence if $\mathbb{V}_1$ and $\mathbb{V}_2$ are elastic symmetry groups, then

$$\mathbb{Z}_2(\mathbb{V}_1) = \mathbb{Z}_2(\mathbb{V}_2) \iff \mathbb{V}_1 = \mathbb{V}_2. \tag{9}$$

A picture of the 2-fold points of $\mathcal{S}_\mathbf{T}$ therefore gives a picture of $\mathcal{S}_\mathbf{T}$; see Fig. 1 of [54]. We also refer to the 2-fold points of $\mathcal{S}_\mathbf{T}$ as the 2-fold points of $\mathbf{T}$ itself.

We let $\mathbb{G}_\Sigma$ be the group of rotations that permute the 2-fold points of $\mathbb{U}_\Sigma$:

$$V \in \mathbb{G}_\Sigma \iff V\big(\mathbb{Z}_2(\mathbb{U}_\Sigma)\big) = \mathbb{Z}_2(\mathbb{U}_\Sigma). \tag{10}$$

Then

$$V \in \mathbb{G}_\Sigma \iff \mathbb{Z}_2(V\mathbb{U}_\Sigma V^\top) = \mathbb{Z}_2(\mathbb{U}_\Sigma) \quad \text{(from Eqs. (10) and (8))}, \tag{11a}$$

$$V \in \mathbb{G}_\Sigma \iff V\mathbb{U}_\Sigma V^\top = \mathbb{U}_\Sigma \quad \text{(from Eq. (9))}. \tag{11b}$$

The groups $\mathbb{G}_\Sigma$ are

$$\begin{aligned} &\mathbb{G}_{\text{ISO}} = \mathbb{G}_{\text{TRIV}} = \mathbb{U}, && \mathbb{G}_{\text{TET}} = \mathbb{D}_8 \ \text{ (see [54])}, \\ &\mathbb{G}_{\text{XISO}} = \mathbb{G}_{\text{MONO}} = \mathbb{U}_{\text{XISO}}, && \mathbb{G}_{\text{TRIG}} = \mathbb{D}_6 \ \text{ (see [54])}, \\ &\mathbb{G}_{\text{ORTH}} = \mathbb{G}_{\text{CUBE}} = \mathbb{U}_{\text{CUBE}}. \end{aligned} \tag{12}$$

To verify Eq. (12) for $\mathbb{G}_{\text{ORTH}}$, for example: The 2-fold points of $\mathbb{U}_{\text{ORTH}}$ are the face centers of the unit cube. The rotations that permute them are the rotations of the unit cube; they make up $\mathbb{U}_{\text{CUBE}}$.

3.1 Regular Angles, Regular Axes

An angle ξ, $0 \le \xi \le \pi$, is said to be regular if $\xi \neq 0,\ \pi/2,\ 2\pi/3,\ \pi$. If V is a symmetry of an elastic map $\mathbf{T}$ and if the rotation angle[1] of V is regular, then any rotation about the rotation axis of V is also a symmetry of $\mathbf{T}$ (Table 2 and Eq. (7)). The axis of V is then said to be a regular axis of $\mathbf{T}$ (or of $\mathcal{S}_\mathbf{T}$), and the two intersections of the axis with the unit sphere are regular points of $\mathbf{T}$.

Theorem 1 says that no elastic symmetry group can properly contain a conjugate of itself.

Theorem 1 *Let $\mathbb{V}$ be an elastic symmetry group. Then*

$$U\mathbb{V}U^\top \subset \mathbb{V} \implies U\mathbb{V}U^\top = \mathbb{V} \qquad (U \in \mathbb{U}). \tag{13}$$

Proof We can assume $\mathbb{V} = \mathbb{U}_\Sigma$.

If $\Sigma \neq$ XISO, then, from Table 2, $\mathbb{V} = \mathbb{U}_{\text{ISO}}$ or $\mathbb{V}$ is finite, and Eq. (13) is correct.

If $\Sigma =$ XISO then $V = \mathbb{U}_{\text{XISO}}$. If also $U\mathbb{V}U^\top \subset \mathbb{V}$, then the regular axes of $U\mathbb{V}U^\top$ and $\mathbb{V}$ coincide, since $\mathbb{V}$ has only one regular axis (Table 2). Then $U\mathbb{V}U^\top = \mathbb{V}$. □

4 The Structure of the Space $\mathcal{T}$ of Elastic Maps

We let $\mathcal{T}$ be the space of all elastic maps, and for each Σ as in Table 1 we let $\mathcal{T}_\Sigma \subset \mathcal{T}$ be the set of elastic maps $\mathbf{T}$ whose symmetry class is at least Σ. More precisely,

$$\mathcal{T}_\Sigma = \left\{\mathbf{T} \in \mathcal{T} : \mathcal{S}_\mathbf{T} \supset U\mathbb{U}_\Sigma U^\top \text{ for some } U \in \mathbb{U}\right\}. \tag{14}$$

For each $U \in \mathbb{U}$ and for each Σ we define a subspace $\boldsymbol{\mathcal{V}}_\Sigma(U)$ of $\mathcal{T}$ by

$$\boldsymbol{\mathcal{V}}_\Sigma(U) = \left\{\mathbf{T} \in \mathcal{T} : \mathcal{S}_\mathbf{T} \supset U\,\mathbb{U}_\Sigma\,U^\top\right\}. \tag{15}$$

From Eqs. (14) and (15),

$$\mathcal{T}_\Sigma = \bigcup_{U \in \mathbb{U}} \boldsymbol{\mathcal{V}}_\Sigma(U). \tag{16}$$

Figure 1 is a (woefully) low-dimensional depiction of $\mathcal{T}_\Sigma$.

Theorem 2

$$\boldsymbol{\mathcal{V}}_\Sigma(U_1) = \boldsymbol{\mathcal{V}}_\Sigma(U_2) \iff U_2 = U_1 G \text{ for some } G \in \mathbb{G}_\Sigma. \tag{17}$$

Proof Suppose $\boldsymbol{\mathcal{V}}_\Sigma(U_1) = \boldsymbol{\mathcal{V}}_\Sigma(U_2)$. Since $U_1\mathbb{U}_\Sigma U_1^\top$ is an elastic symmetry group, there is $\mathbf{T} \in \mathcal{T}$ such that $\mathcal{S}_\mathbf{T} = U_1\mathbb{U}_\Sigma U_1^\top$. Then $\mathbf{T} \in \boldsymbol{\mathcal{V}}_\Sigma(U_1) = \boldsymbol{\mathcal{V}}_\Sigma(U_2)$ and so

$$U_1\mathbb{U}_\Sigma U_1^\top = \mathcal{S}_\mathbf{T} \supset U_2\mathbb{U}_\Sigma U_2^\top.$$

Then $U_1\mathbb{U}_\Sigma U_1^\top = U_2\mathbb{U}_\Sigma U_2^\top$ from Theorem 1. Then $U_1^\top U_2 \in \mathbb{G}_\Sigma$ from Eq. (11b), and so $U_2 = U_1 G$ for some $G \in \mathbb{G}_\Sigma$.

The converse is from Eqs. (15) and (11b). □

[1] The rotation angle ξ of V is characterized by $\cos\xi = \dfrac{-1 + \text{tr}(V)}{2}$, $0 \le \xi \le \pi$.

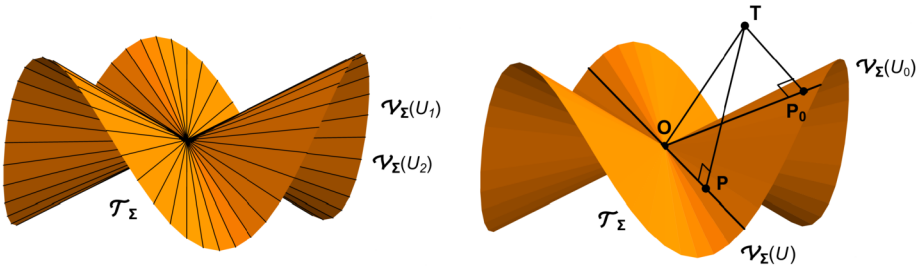

Fig. 1 (*Left*) Rudimentary depiction of the set $\mathcal{T}_\Sigma$ (orange) of elastic maps having symmetry at least Σ (Eq. 14). The diagram is so idealized that it should not be taken too seriously, but it reminds us that although for $\Sigma \neq \text{ISO}, \text{TRIV}$, the set $\mathcal{T}_\Sigma$ is not itself a subspace of $\mathcal{T}$, it is the union of the subspaces $\mathcal{V}_\Sigma(U)$, $U \in \mathbb{U}$. Here each subspace $\mathcal{V}_\Sigma(U)$ is shown as a line through the origin. (*Right*) The orthogonal projection $\mathbf{P}$ of an elastic map $\mathbf{T}$ to $\mathcal{V}_\Sigma(U)$. Although $\mathbf{P}$ is the closest point to $\mathbf{T}$ in $\mathcal{V}_\Sigma(U)$, it is not the closest point to $\mathbf{T}$ in $\mathcal{T}_\Sigma$; that point is $\mathbf{P}_0$. The dimensions in the diagrams are unrealistically low. For $\Sigma = \text{ORTH}$, for example, the dimension of each subspace $\mathcal{V}_\Sigma(U)$ would be 9 and the dimension of $\mathcal{T}_\Sigma$ would be 12. Both diagrams are misleading when $\Sigma = \text{ISO}$ or $\Sigma = \text{TRIV}$, since $\mathcal{V}_{\text{ISO}}(U) = \mathcal{T}_{\text{ISO}}$ is a two-dimensional subspace, independent of U, and $\mathcal{V}_{\text{TRIV}}(U) = \mathcal{T}_{\text{TRIV}} = \mathcal{T}$, again independent of U. The subspaces $\mathcal{V}_\Sigma(U)$ are not so nearly disjoint as the diagram suggests; from Eq. (15) the subspace $\mathcal{T}_{\text{ISO}}$ is common to all of them.

From Eq. (15) we find $\mathcal{V}_{\text{ISO}}(I) \subset \mathcal{V}_\Sigma(U)$ (any Σ, any $U \in \mathbb{U}$). Hence from Eq. (4),

$$\mathbf{P}\Big(\mathbf{P}\big(\mathbf{T}, \mathcal{V}_\Sigma(U)\big), \mathcal{V}_{\text{ISO}}(I)\Big) = \mathbf{P}\left(\mathbf{T}, \mathcal{V}_{\text{ISO}}(I)\right). \tag{18}$$

Equation (18) becomes more transparent if we define $\mathbf{P}_{\text{ISO}}$ to be the projection mapping onto $\mathcal{V}_{\text{ISO}}(I)$. Then

$$\mathbf{P}_{\text{ISO}}\Big(\mathbf{P}\big(\mathbf{T}, \mathcal{V}_\Sigma(U)\big)\Big) = \mathbf{P}_{\text{ISO}}(\mathbf{T}) \qquad (U \in \mathbb{U}, \text{ any } \Sigma). \tag{19}$$

From Eqs. (15) and (6),

$$\mathcal{V}_\Sigma(U) = \overline{U} \circ \mathcal{V}_\Sigma(I) \circ \overline{U}^*, \tag{20}$$

where the subspace on the right consists of all elastic maps of the form $\overline{U} \circ \mathbf{T} \circ \overline{U}^*$, $\mathbf{T} \in \mathcal{V}_\Sigma(I)$.

4.1 The Functions $\alpha^{\mathbf{T}}_{\text{MONO}}$ and $\alpha^{\mathbf{T}}_{\text{XISO}}$

From Eq. (15) the subspace $\mathcal{V}_{\text{MONO}}(U)$ consists of the elastic maps that have $\mathbf{v} = U\mathbf{k}$ as a 2-fold point, and $\mathcal{V}_{\text{XISO}}(U)$ consists of the elastic maps that have $\mathbf{v} = U\mathbf{k}$ as a regular point. We can therefore consider $\mathcal{V}_{\text{MONO}}(U)$ and $\mathcal{V}_{\text{XISO}}(U)$ as functions of points $\mathbf{v} \in \mathbb{S}^2$ rather than as functions of matrices $U \in \mathbb{U}$. We thus abuse the notation a bit and let

$$\mathcal{V}_{\text{MONO}}(\mathbf{v}) = \mathcal{V}_{\text{MONO}}(Z_\theta Y_\phi), \tag{21a}$$

$$\mathcal{V}_{\text{XISO}}(\mathbf{v}) = \mathcal{V}_{\text{XISO}}(Z_\theta Y_\phi), \tag{21b}$$

where (θ, ϕ) are the spherical coordinates of $\mathbf{v}$. (Thus $Z_\theta Y_\phi \mathbf{k} = \mathbf{v}$.) For an elastic map $\mathbf{T}$, its "monoclinic angle" at $\mathbf{v}$ is then defined to be

$$\alpha^{\mathbf{T}}_{\text{MONO}}(\mathbf{v}) = \angle\left(\mathbf{T}, \mathbf{P}(\mathbf{T}, \mathcal{V}_{\text{MONO}}(\mathbf{v}))\right) = \cos^{-1}\frac{\|\mathbf{P}(\mathbf{T}, \mathcal{V}_{\text{MONO}}(\mathbf{v}))\|}{\|\mathbf{T}\|}, \tag{22a}$$

the second equality being from Eq. (3). The number $\alpha^{\mathbf{T}}_{\text{MONO}}(\mathbf{v})$ is a measure of how far $\mathbf{T}$ is from having a 2-fold point at $\mathbf{v}$. In particular, $\alpha^{\mathbf{T}}_{\text{MONO}}(\mathbf{v}) = 0$ if and only if $\mathbf{v}$ is a 2-fold point of $\mathbf{T}$. The function $\alpha^{\mathbf{T}}_{\text{MONO}}$ is closely related to the monoclinic distance function [19, 54], but $\alpha^{\mathbf{T}}_{\text{MONO}}$ differs by being independent of $\|\mathbf{T}\|$.

In later figures we will depict elastic maps as contour plots of their monoclinic angle functions on $\mathbb{S}^2$. The plot of $\alpha^{\mathbf{T}}_{\text{MONO}}$ will have all the symmetries of $\mathbf{T}$ [54, Theorem 2]. We conjectured in [54] that the converse would be true as well, that is, that the (rotational) symmetries of $\alpha^{\mathbf{T}}_{\text{MONO}}$ would also be symmetries of $\mathbf{T}$. There turn out to be elastic maps, however, for which this fails.[2] It is a reminder that the zero contour of $\alpha^{\mathbf{T}}_{\text{MONO}}$, rather than the symmetries of $\alpha^{\mathbf{T}}_{\text{MONO}}$, has the final say in determining the symmetry group of $\mathbf{T}$.

Since 2-fold points come in antipodal pairs, then $\boldsymbol{\mathcal{V}}_{\text{MONO}}(\mathbf{v}) = \boldsymbol{\mathcal{V}}_{\text{MONO}}(-\mathbf{v})$. Hence the antipodal map $\mathbf{v} \to -\mathbf{v}$ is a (non-rotational) symmetry of $\alpha^{\mathbf{T}}_{\text{MONO}}$.

Similarly to Eq. (22a), the XISO angle of $\mathbf{T}$ at $\mathbf{v}$ is defined by

$$\alpha^{\mathbf{T}}_{\text{XISO}}(\mathbf{v}) = \angle\left(\mathbf{T},\, \mathbf{P}(\mathbf{T}, \boldsymbol{\mathcal{V}}_{\text{XISO}}(\mathbf{v}))\right). \tag{22b}$$

It measures how far $\mathbf{T}$ is from having a regular point at $\mathbf{v}$.

For a given $\mathbf{v} \in \mathbb{S}^2$ the condition $U\mathbf{k} = \mathbf{v}$ is satisfied by any rotation matrix U whose third column is $\mathbf{v}$. Of these, the one that swaps $\mathbf{k}$ and $\mathbf{v}$, is, if $\mathbf{v} \neq \pm\mathbf{k}$,

$$U_{\mathbf{v}} = \frac{1}{1+z}\begin{pmatrix} -y^2 - z(1+z) & xy & x(1+z) \\ xy & -x^2 - z(1+z) & y(1+z) \\ x(1+z) & y(1+z) & z(1+z) \end{pmatrix} \qquad \big(\mathbf{v} = (x, y, z) \in \mathbb{S}^2\big). \tag{23}$$

5 Calculating the Projection to $\boldsymbol{\mathcal{V}}_{\boldsymbol{\Sigma}}(U)$

In Appendix C.1 we use Eq. (20) to show that for any subspace $\boldsymbol{\mathcal{V}}$ of $\boldsymbol{\mathcal{T}}$ and for $U \in \mathbb{U}$,

$$\mathbf{P}\big(\mathbf{T},\, \overline{U} \circ \boldsymbol{\mathcal{V}} \circ \overline{U}^*\big) = \overline{U} \circ \mathbf{P}\big(\mathbf{A}, \boldsymbol{\mathcal{V}}\big) \circ \overline{U}^*, \tag{24a}$$

where

$$\mathbf{A} = \mathbf{A}(\mathbf{T}, U) = \overline{U}^* \circ \mathbf{T} \circ \overline{U}. \tag{24b}$$

Taking $\boldsymbol{\mathcal{V}} = \boldsymbol{\mathcal{V}}_{\Sigma}(I)$ in Eq. (24a) gives

$$\mathbf{P}\big(\mathbf{T}, \boldsymbol{\mathcal{V}}_{\Sigma}(U)\big) = \overline{U} \circ \mathbf{P}\big(\mathbf{A}, \boldsymbol{\mathcal{V}}_{\Sigma}(I)\big) \circ \overline{U}^*. \tag{25}$$

The inner product of $n \times n$ matrices $M = (m_{ij})$ and $N = (n_{ij})$ is defined by

$$M \cdot N = \sum_{i,\,j\,=\,1}^{n} m_{ij}\, n_{ij}. \tag{26}$$

(Juxtaposition of matrices, with no dot, signifies matrix multiplication.) For any elastic map $\mathbf{T}$, we let $[\mathbf{T}] = [\mathbf{T}]_{\mathbb{B}\mathbb{B}}$ be the matrix (representation) of $\mathbf{T}$ with respect to the orthonormal

[2] If the non-zero entries of $[\mathbf{T}]_{\mathbb{B}\mathbb{B}} = T = (t_{ij})$ are 1, 2, 3, 4, 5, 6 down the main diagonal, together with $t_{36} = t_{63} = 1$, then $V = I, X_\pi, Y_\pi, Z_\pi$ are symmetries of $\alpha^{\mathbf{T}}_{\text{MONO}}$. That is, $\alpha^{\mathbf{T}}_{\text{MONO}}(V\mathbf{v}) = \alpha^{\mathbf{T}}_{\text{MONO}}(\mathbf{v})$ for all $\mathbf{v} \in \mathbb{S}^2$. The only symmetries of $\mathbf{T}$, however, are I and Z_π.

basis $\mathbb{B}$ given in Eq. (80). The inner product of elastic maps $\mathbf{T}_1$ and $\mathbf{T}_2$ is then defined[3] via their matrices:

$$\mathbf{T}_1 \cdot \mathbf{T}_2 = [\mathbf{T}_1] \cdot [\mathbf{T}_2]\,. \tag{27}$$

We define $\mathcal{T}$ to consist of the matrices of all elastic maps. We likewise define $\mathcal{V}_\Sigma^{\mathbb{B}}(U)$ to consist of the matrices, with respect to $\mathbb{B}$, of elastic maps in $\boldsymbol{\mathcal{V}}_\Sigma(U)$:

$$\mathcal{T} = \{[\mathbf{T}] : \mathbf{T} \in \boldsymbol{\mathcal{T}}\}, \tag{28}$$

$$\mathcal{V}_\Sigma^{\mathbb{B}}(U) = \{[\mathbf{T}] : \mathbf{T} \in \boldsymbol{\mathcal{V}}_\Sigma(U)\}\,. \tag{29}$$

We let $P(T, \mathcal{V}_\Sigma^{\mathbb{B}}(U))$ be the orthogonal projection of $T \in \mathcal{T}$ to $\mathcal{V}_\Sigma^{\mathbb{B}}(U)$. Then from Appendix C.2,

$$\big[\mathbf{P}\big(\mathbf{T}, \boldsymbol{\mathcal{V}}_\Sigma(U)\big)\big] = P(T, \mathcal{V}_\Sigma^{\mathbb{B}}(U)) \qquad (T = [\mathbf{T}]). \tag{30}$$

That is, the matrix of the projection is the projection of the matrix. Equations (25) and (30) then give

$$\big[\mathbf{P}\big(\mathbf{T}, \boldsymbol{\mathcal{V}}_\Sigma(U)\big)\big] = [\overline{U}]\, P\big(A, \mathcal{V}_\Sigma^{\mathbb{B}}(I)\big)\, [\overline{U}]^\top, \tag{31a}$$

$$A = A(T, U) = [\overline{U}]^\top T\, [\overline{U}]. \tag{31b}$$

The matrix $\big[\overline{U}\big]$ is [53, Eq. 59b]

$$\big[\overline{U}\big] = \big[\overline{U}\big]_{\mathbb{B}\mathbb{B}} = \begin{pmatrix} (U B_1 U^\top) \cdot B_1 & \dots & (U B_6 U^\top) \cdot B_1 \\ \vdots & & \vdots \\ (U B_1 U^\top) \cdot B_6 & \dots & (U B_6 U^\top) \cdot B_6 \end{pmatrix}, \tag{32}$$

The matrix of $\mathbf{P}\big(\mathbf{T}, \boldsymbol{\mathcal{V}}_\Sigma(U)\big)$ is then calculated from Eqs. (31a), (31b), (32), (84a)–(84h).

The distance from $\mathbf{T}$ to $\mathbf{P}(\mathbf{T}, \boldsymbol{\mathcal{V}}_\Sigma(U))$ is

$$\begin{aligned} d(\mathbf{T}, \boldsymbol{\mathcal{V}}_\Sigma(U)) &= \Big\| \mathbf{T} - \mathbf{P}\big(\mathbf{T}, \boldsymbol{\mathcal{V}}_\Sigma(U)\big) \Big\| \\ &= \big\| [\overline{U}]\, A\, [\overline{U}]^\top - [\overline{U}]\, P\big(A, \mathcal{V}_\Sigma^{\mathbb{B}}(I)\big)\, [\overline{U}]^\top \big\| \qquad \text{(from Eq. (31a) and (31b))} \\ &= \big\| A - P\big(A, \mathcal{V}_\Sigma^{\mathbb{B}}(I)\big) \big\|\,. \end{aligned} \tag{33}$$

[3] Any orthonormal basis $\mathbb{B}'$ can replace $\mathbb{B}$ in the definition, since

$$[\mathbf{T}_1]_{\mathbb{B}'\mathbb{B}'} \cdot [\mathbf{T}_2]_{\mathbb{B}'\mathbb{B}'} = [\mathbf{T}_1]_{\mathbb{B}\mathbb{B}} \cdot [\mathbf{T}_2]_{\mathbb{B}\mathbb{B}}.$$

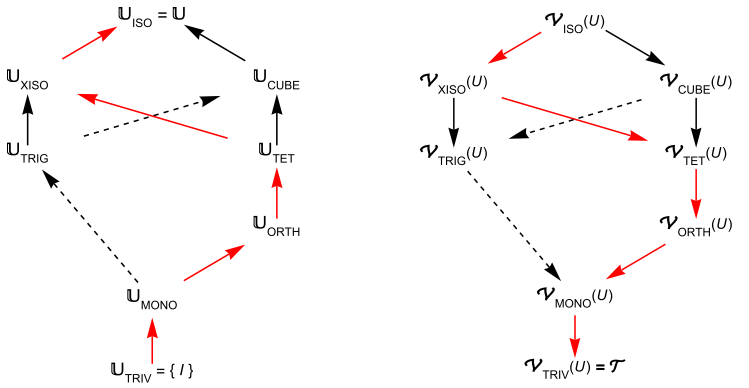

Fig. 2 (*Left*) Inclusion relations among the reference groups for elastic symmetry. A solid arrow from one group to another indicates that the first group is a subgroup of the second. A dashed arrow only means that a conjugate of the first group is a subgroup of the second. The subgroup relations follow from Table 2. (*Right*) Inclusion relations among the Σ subspaces $\boldsymbol{\mathcal{V}}_{\Sigma}(U)$ of $\boldsymbol{\mathcal{T}}$. Again the solid arrows indicate true inclusions. The inclusions follow from Eq. (15). The red path is the path chosen by Browaeys & Chevrot [9] (our Eqs. (34a) and (34b)).

6 The Decomposition

As in Fig. 2,

$$\boldsymbol{\mathcal{T}}_{\mathrm{ISO}} = \boldsymbol{\mathcal{V}}_{\Sigma_1}(U) \subset \cdots \subset \boldsymbol{\mathcal{V}}_{\Sigma_6}(U) = \boldsymbol{\mathcal{T}}, \tag{34a}$$

where

$$\Sigma_1 = \mathrm{ISO},\ \Sigma_2 = \mathrm{XISO},\ \Sigma_3 = \mathrm{TET},\ \Sigma_4 = \mathrm{ORTH},\ \Sigma_5 = \mathrm{MONO},\ \Sigma_6 = \mathrm{TRIV}. \tag{34b}$$

Equation (35), next, is based on Walker & Wookey [58], which is meant to implement Browaeys & Chevrot [9]. For a given elastic map $\mathbf{T}$ and a given rotation matrix U, we define what will be the k^{th} summand of $\mathbf{T}$ by

$$\mathbf{Q}_{\Sigma_k}(\mathbf{T}, U) = \mathbf{P}\left(\mathbf{T},\ \boldsymbol{\mathcal{V}}_{\Sigma_k}(U)\right) - \mathbf{P}\left(\mathbf{T},\ \boldsymbol{\mathcal{V}}_{\Sigma_{k-1}}(U)\right), \tag{35}$$

where Σ_k is as in Eq. (34b). Although Σ_0 itself has no meaning, we agree to define

$$\boldsymbol{\mathcal{V}}_{\Sigma_0}(U) = \{\mathbf{0}\} \subset \boldsymbol{\mathcal{T}}, \tag{36}$$

so that Eq. (35) makes sense for $k = 1$, as well as for $k = 2, \ldots, 6$.

Theorem 3 (The decomposition) *Let* $\mathbf{T}$ *be an elastic map and* $U \in \mathbb{U}$. *Then*

$$\mathbf{T} = \sum_{k=1}^{6} \mathbf{Q}_{\Sigma_k}(\mathbf{T}, U), \tag{37a}$$

$$\mathbf{Q}_{\Sigma_k}(\mathbf{T}, U) \in \boldsymbol{\mathcal{V}}_{\Sigma_k}(U) \cap \left(\boldsymbol{\mathcal{V}}_{\Sigma_{k-1}}(U)\right)^{\perp}. \tag{37b}$$

Proof For purposes of the proof, we abbreviate $\mathbf{Q}_{\Sigma_k}(\mathbf{T}, U)$ and $\boldsymbol{\mathcal{V}}_{\Sigma_k}(U)$ to $\mathbf{Q}_k$ and $\boldsymbol{\mathcal{V}}_k$. From Eq. (35),

$$\sum_{j=1}^{k} \mathbf{Q}_j = \mathbf{P}(\mathbf{T},\, \boldsymbol{\mathcal{V}}_k)\,. \tag{38}$$

$$\mathbf{T} \in \boldsymbol{\mathcal{V}}_k \iff \mathbf{T} = \mathbf{P}(\mathbf{T}, \boldsymbol{\mathcal{V}}_k) \qquad \text{(from Eq. (1a))}, \tag{39a}$$

$$\mathbf{T} \in \boldsymbol{\mathcal{V}}_k \iff \mathbf{T} = \sum_{j=1}^{k} \mathbf{Q}_j \qquad \text{(from Eq. (38))}. \tag{39b}$$

Since $\mathbf{T} \in \boldsymbol{\mathcal{T}} = \boldsymbol{\mathcal{V}}_{\text{TRIV}}(U) = \boldsymbol{\mathcal{V}}_6$, regardless of U, this proves Eq. (37a).

From Eq. (35) and then from Eq. (1a),

$$\mathbf{Q}_k = \underbrace{\mathbf{P}(\mathbf{T},\, \boldsymbol{\mathcal{V}}_k)}_{\in \boldsymbol{\mathcal{V}}_k} - \underbrace{\mathbf{P}(\mathbf{T},\, \boldsymbol{\mathcal{V}}_{k-1})}_{\in \boldsymbol{\mathcal{V}}_{k-1}} \in \boldsymbol{\mathcal{V}}_k. \tag{40a}$$

Similarly, from Eq. (35) and then from Eq. (1b),

$$\mathbf{Q}_k = -\underbrace{\big(\mathbf{T} - \mathbf{P}(\mathbf{T},\, \boldsymbol{\mathcal{V}}_k)\big)}_{\in \boldsymbol{\mathcal{V}}_k^{\perp}} + \underbrace{\mathbf{T} - \mathbf{P}(\mathbf{T},\, \boldsymbol{\mathcal{V}}_{k-1})}_{\in \boldsymbol{\mathcal{V}}_{k-1}^{\perp}} \in \boldsymbol{\mathcal{V}}_{k-1}^{\perp}. \tag{40b}$$

Together, Eqs. (40a) and (40b) prove Eq. (37b). □

If $\mathbf{T} \in \boldsymbol{\mathcal{V}}_{\Sigma_k}(U)$ and $j \geq k$, then $\mathbf{T} \in \boldsymbol{\mathcal{V}}_{\Sigma_j}(U)$ and so $\mathbf{P}(\mathbf{T}, \boldsymbol{\mathcal{V}}_{\Sigma_j}(U)) = \mathbf{T}$. Hence $\mathbf{Q}_{\Sigma_j}(\mathbf{T}, U) = \mathbf{0}$ for $j > k$, so that the decomposition for $\mathbf{T}$ and U essentially terminates at the k^{th} summand. If, for example, $\mathbf{T} \in \boldsymbol{\mathcal{V}}_{\text{TET}}(U)$, then

$$\mathbf{T} = \mathbf{Q}_{\text{ISO}}(\mathbf{T}, U) + \mathbf{Q}_{\text{XISO}}(\mathbf{T}, U) + \mathbf{Q}_{\text{TET}}(\mathbf{T}, U). \tag{41}$$

In Appendix C.3 we show that for any elastic maps $\mathbf{Q}_1, \ldots, \mathbf{Q}_6$,

$$\left.\begin{aligned} \mathbf{T} &= \sum_{k=1}^{6} \mathbf{Q}_k \\ \mathbf{Q}_k &\in \boldsymbol{\mathcal{V}}_{\Sigma_k}(U) \cap \big(\boldsymbol{\mathcal{V}}_{\Sigma_{k-1}}(U)\big)^{\perp} \end{aligned}\right\} \implies \mathbf{Q}_k = \mathbf{Q}_{\Sigma_k}(\mathbf{T}, U). \tag{42}$$

Equation (42) is thus the converse to Theorem 3. It guarantees that for a given $\mathbf{T}$ and U the hypotheses of Eq. (42) determine the decomposition uniquely. In the literature the decomposition is sometimes described as satisfying $\mathbf{T} = \sum_{k=1}^{6} \mathbf{Q}_k$, $\mathbf{Q}_k \in \boldsymbol{\mathcal{V}}_{\Sigma_k}(U)$, and $\mathbf{Q}_j \cdot \mathbf{Q}_k = 0$ for $j \neq k$. That is true, but those three conditions do not determine the decomposition.

7 Hexagonal Approximation of $\mathbf{T}$

In our terms, hexagonal approximation is transverse isotropic approximation, abbreviated XISO-approximation.

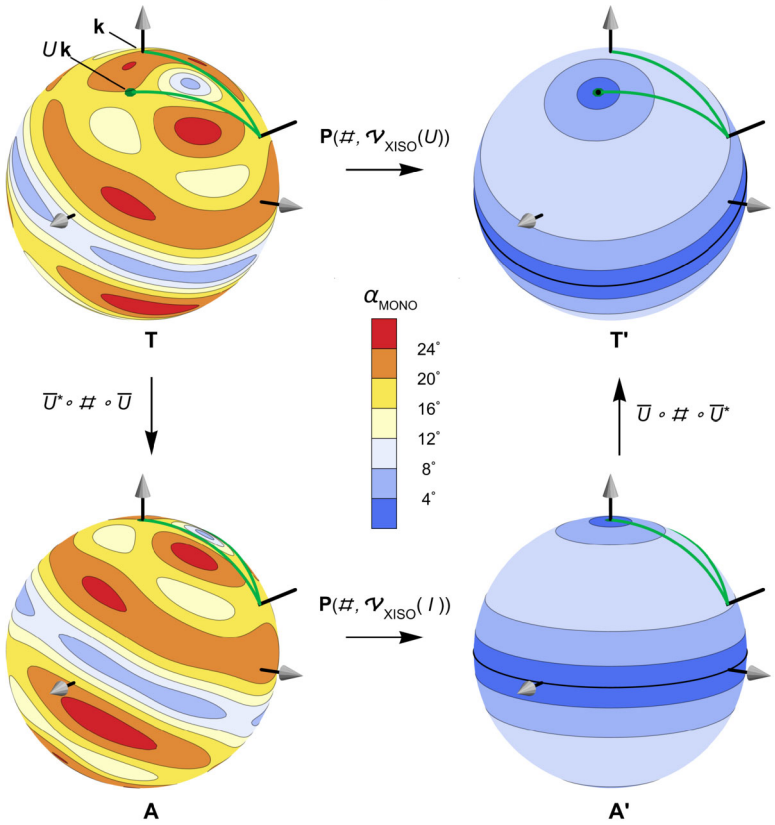

Fig. 3 A poor XISO-approximation $\mathbf{T}'$ for the given elastic map $\mathbf{T}$. Each of the elastic maps $\mathbf{T}$, $\mathbf{T}'$, $\mathbf{A}$, $\mathbf{A}'$ is represented by the contour plot of its monoclinic angle function (Eq. 22a). The plots for $\mathbf{A}$ and $\mathbf{A}'$ differ from those for $\mathbf{T}$ and $\mathbf{T}'$ by $U^{\top}$, which is a rotation of 37° about the axis seen protruding from each sphere. (From this perspective the rotation is clockwise.) The calculation of $\mathbf{T}'$ from $\mathbf{T}$ follows the path $\mathbf{T} \to \mathbf{A} \to \mathbf{A}' \to \mathbf{T}'$ (Eq. (24a) and (24b)). The dissimilarity of the plots for $\mathbf{T}$ and $\mathbf{T}'$ confirms that $\mathbf{T}' = \mathbf{X}(\mathbf{T}, U)$ is a poor approximation for $\mathbf{T}$. The failure of the approximation is due to a poor choice of the rotation matrix U.

In their Sect. 4.5, Hexagonal Approximation, Browaeys & Chevrot [9] talk about the "optimum equivalent hexagonal medium" for an elastic map, but they do not say what they mean.

For a given elastic map $\mathbf{T}$, Browaeys and Chevrot conceivably meant the XISO-approximation to be $\mathbf{Q}_{\text{XISO}}(\mathbf{T}, U)$. The elastic map $\mathbf{Q}_{\text{XISO}}(\mathbf{T}, U)$, however, is never physically permissible (our Sect. 12.3).

They might also have meant the XISO-approximation to be $\mathbf{Q}_{\text{ISO}}(\mathbf{T}, U) + \mathbf{Q}_{\text{XISO}}(\mathbf{T}, U)$; this is what Becker et al [3, Eq. 2] use. We follow them and, using Eq. (38), we define the XISO-approximation $\mathbf{X}(\mathbf{T}, U)$ by

$$\mathbf{X}(\mathbf{T}, U) = \mathbf{P}\left(\mathbf{T},\ \boldsymbol{\mathcal{V}}_{\text{XISO}}(U)\right). \tag{43}$$

Then $\mathbf{X}(\mathbf{T}, U)$ is in $\boldsymbol{\mathcal{V}}_{\text{XISO}}(U)$ and hence has $U\mathbf{k}$ as a regular axis.

Figure 3, to be discussed next, shows an instance where $\mathbf{X}(\mathbf{T}, U)$ fails badly as an XISO-approximation to $\mathbf{T}$.

We depict each elastic map $\mathbf{R}$ as the contour plot on $\mathbb{S}^2$ of its monoclinic angle function $\alpha^{\mathbf{R}}_{\text{MONO}}$ (Eq. (22a)). Recall from Sect. 4.1 that the zero contour of $\alpha^{\mathbf{R}}_{\text{MONO}}$ consists of the 2-fold points of $\mathbf{R}$. If the symmetry class of $\mathbf{R}$ is transverse isotropic, the contours of $\alpha^{\mathbf{R}}_{\text{MONO}}$ are circles covering $\mathbb{S}^2$, all with poles at the two regular points of $\mathbf{R}$. The great circle, together with its two poles, make up the zero-contour of $\alpha^{\mathbf{R}}_{\text{MONO}}$.

Figure 3 is Eq. (24a) in pictures. The top path $\mathbf{T} \to \mathbf{T}'$ in the figure is the left side of the equation, and the path $\begin{matrix}\mathbf{T} & \mathbf{T}' \\ \downarrow & \uparrow \\ \mathbf{A} & \longrightarrow \mathbf{A}'\end{matrix}$ is the right side. With $\mathbf{T}$ and U as in Appendix D, the four elastic maps are

$$\begin{aligned} &\mathbf{T} \text{ (given)}, && \mathbf{T}' = \mathbf{X}(\mathbf{T}, U), \\ &\mathbf{A} = \mathbf{A}(\mathbf{T}, U), && \mathbf{A}' = \mathbf{X}(\mathbf{A},\, I\,), \end{aligned} \tag{44}$$

where $\mathbf{A}(\mathbf{T}, U)$ is from Eq. (24b). Thus $\mathbf{T}'$ is the XISO-approximation to $\mathbf{T}$. Note that the arrow from $\mathbf{A}$ to $\mathbf{A}'$ in Fig. 3 is projection to $\boldsymbol{\mathcal{V}}_{\text{XISO}}(I)$ rather than to $\boldsymbol{\mathcal{V}}_{\text{XISO}}(U)$, so $\mathbf{A}'$ is easily calculated from $\mathbf{A}$ using Eq. (84b).

The plot for $\mathbf{A}$ (i.e., the plot of $\alpha^{\mathbf{A}}_{\text{MONO}}$) differs from that for $\mathbf{T}$ by the rotation $U^\top$, which is a rotation of 37° about the axis seen protruding from the sphere. The plots for $\mathbf{A}$ and $\mathbf{A}'$ are related as follows. The subspace $\boldsymbol{\mathcal{V}}_{\text{XISO}}(I)$ consists of all elastic maps whose matrix representations are XISO reference matrices $T^{\mathbb{B}}_{\text{XISO}}(a, c, e, f, k)$ (Eq. (82)). Their regular axes are vertical, so the contours of $\alpha^{\mathbf{A}'}_{\text{MONO}}$ must be horizontal circles. In finding $\mathbf{A}'$ from $\mathbf{A}$, the projection gives the values of a, c, e, f, k that minimize the distance from $A = [\mathbf{A}]_{\mathbb{BB}}$ to $T^{\mathbb{B}}_{\text{XISO}}(a, c, e, f, k)$; this determines the values on the circles.

In this example the plot for $\mathbf{T}$ (Fig. 3, upper left), with its prominent bluish band together with the bluish patch 90° from it ($\alpha^{\mathbf{T}}_{\text{MONO}}$ is small on both), resembles a distorted plot of an XISO-map. We would thus expect the XISO-approximation to resemble $\mathbf{T}$, but that would have required that the bluish band in the plot for $\mathbf{A}$ be more or less horizontal. It is not, and so $T^{\mathbb{B}}_{\text{XISO}}(a, c, e, f, k)$ cannot be made close to A. As a result, the plot for $\mathbf{A}'$ looks nothing like that for $\mathbf{A}$. The plot for the XISO-approximation $\mathbf{T}'$, which differs from that for $\mathbf{A}'$ by the rotation U, then looks nothing like that for $\mathbf{T}$.

The fault thus lies with the rotation matrix U. Since $U\mathbf{k}$ in the plot for $\mathbf{T}$ gets mapped to $\mathbf{k}$ in the plot for $\mathbf{A}$, the point $U\mathbf{k}$ would need to have been in the small bluish patch (or its antipodal patch) in order to get a good XISO-approximation to $\mathbf{T}$.

8 Closest Σ-Map to T

Since the set $\boldsymbol{\mathcal{T}}_\Sigma$ of elastic maps with symmetry at least Σ is the union of the subspaces $\boldsymbol{\mathcal{V}}_\Sigma(U)$, $U \in \mathbb{U}$, then the distance from an elastic map $\mathbf{T}$ to $\boldsymbol{\mathcal{T}}_\Sigma$ is

$$d(\mathbf{T}, \boldsymbol{\mathcal{T}}_\Sigma) = \min_{U \in \mathbb{U}} d(\mathbf{T}, \boldsymbol{\mathcal{V}}_\Sigma(U)). \tag{45}$$

If U is a rotation matrix where the minimum is realized, then U is said to be a Σ-minimizer for $\mathbf{T}$:

$$U \text{ is a } \Sigma\text{-minimizer for } \mathbf{T} \iff d\,(\mathbf{T}, \boldsymbol{\mathcal{V}}_\Sigma(U)) = \min_{V \in \mathbb{U}} d(\mathbf{T}, \boldsymbol{\mathcal{V}}_\Sigma(V)). \tag{46}$$

Hence U is a Σ-minimizer for $\mathbf{T}$ if and only if

$$d\big(\mathbf{T},\, \mathbf{P}(\mathbf{T}, \boldsymbol{\mathcal{V}}_\Sigma(U))\big) = d(\mathbf{T}, \boldsymbol{\mathcal{T}}_\Sigma). \tag{47}$$

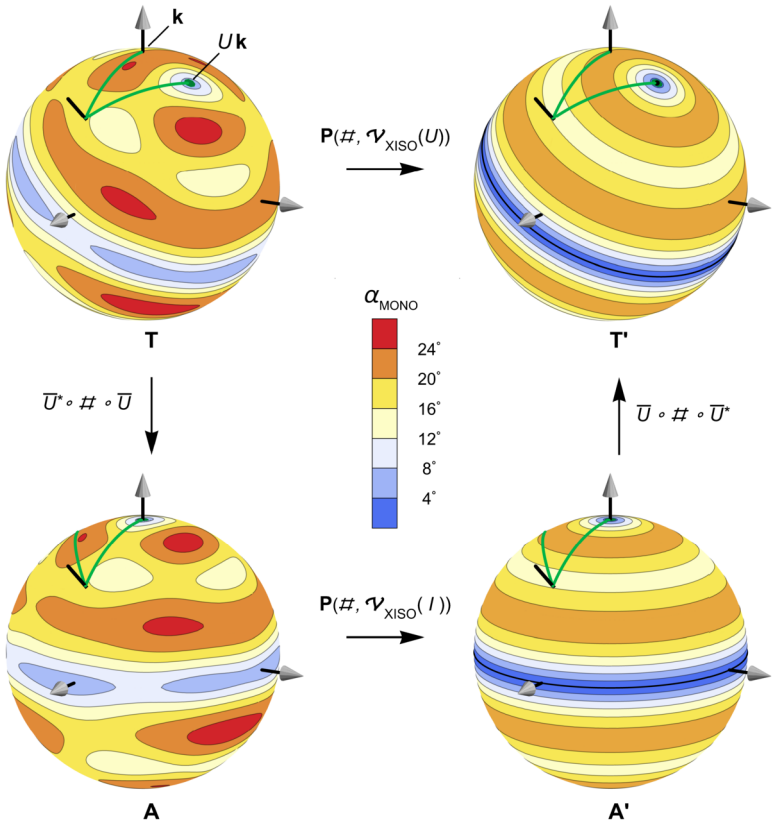

Fig. 4 Same as Fig. 3 but with a better choice of the rotation matrix U. Here in fact U is the XISO-minimizer in Eq. (95); it makes $\mathbf{T}' = \mathbf{P}(\mathbf{T}, \boldsymbol{\mathcal{V}}_{\mathrm{XISO}}(U))$ the closest XISO-map to $\mathbf{T}$. Compare the similarity of the plots for $\mathbf{T}$ and $\mathbf{T}'$ here with the dissimilarity in Fig. 3. The key feature in the present figure is that $U\mathbf{k}$ in the plot for $\mathbf{T}$ is in the small bluish patch, which is a pseudo-pole for the bluish band. Since $U^\top$ maps $U\mathbf{k}$ to $\mathbf{k}$, the bluish band in the plot for $\mathbf{A}$ ends up horizontal. The matrices for $\mathbf{T}$ and $\mathbf{T}'$ are given in Eqs. (93) and (96) and can be seen to be close.

In that case $\mathbf{P}(\mathbf{T}, \boldsymbol{\mathcal{V}}_\Sigma(U))$ is a closest elastic map in $\boldsymbol{\mathcal{T}}_\Sigma$ to $\mathbf{T}$. In Fig. 1, the rotation matrix U_0 would be a Σ-minimizer for $\mathbf{T}$, and the point $\mathbf{P}_0$ would represent the closest elastic map in $\boldsymbol{\mathcal{T}}_\Sigma$ to $\mathbf{T}$.

Figure 4 is like Fig. 3 but with the rotation matrix in Fig. 4 being an XISO-minimizer for $\mathbf{T}$, so that $\mathbf{T}'$ is now a closest XISO-map to $\mathbf{T}$. The plot for $\mathbf{T}'$ in Fig. 4 indeed resembles the plot for $\mathbf{T}$.

8.1 Finding a Σ-Minimizer

To perform the minimization in Eq. (46), we first parameterize $\mathbb{U}$ using the function

$$(\theta, \sigma, \phi) \to \widehat{U}_{(\theta,\sigma,\phi)} = Z_\theta Y_\phi Z_\sigma. \tag{48}$$

We then minimize

$$d\big(\mathbf{T}, \boldsymbol{\mathcal{V}}_\Sigma(\widehat{U}_{(\theta,\sigma,\phi)})\big), \quad 0 \le \theta \le 2\pi,\ |\sigma| \le \pi,\ 0 \le \phi \le \pi, \tag{49}$$

where $d\big(\mathbf{T}, \boldsymbol{\mathcal{V}}_\Sigma(U)\big)$ is given by Eq. (33). (Smaller domains are possible, due to Eq. (17)). The minimization will normally require numerical rather than analytic treatment. We use the Mathematica routine `NMinimize`, supplemented with various independent checks. Our Mathematica code is as per the Code Availability section.

9 $\Sigma_\mathbf{T}$-Minimizers for T

We let $\Sigma_\mathbf{T}$ denote the symmetry class of $\mathbf{T}$. That is, the symmetry group $\mathcal{S}_\mathbf{T}$ is $V\mathbb{U}_{\Sigma_\mathbf{T}}V^\top$ for some $V \in \mathbb{U}$. Then $\mathbf{T} \in \boldsymbol{\mathcal{T}}_{\Sigma_\mathbf{T}}$.

If U is a $\Sigma_\mathbf{T}$-minimizer for $\mathbf{T}$, then

$$\begin{aligned} 0 = d(\mathbf{T}, \boldsymbol{\mathcal{T}}_{\Sigma_\mathbf{T}}) = d(\mathbf{T}, \boldsymbol{\mathcal{V}}_{\Sigma_\mathbf{T}}(U)) \qquad & \text{(Eq. (46))}, \\ \mathbf{T} \in \boldsymbol{\mathcal{V}}_{\Sigma_\mathbf{T}}(U), \qquad & \\ \mathcal{S}_\mathbf{T} \supset U\mathbb{U}_{\Sigma_\mathbf{T}}U^\top \qquad & \text{(Eq. (15))}, \\ \mathcal{S}_\mathbf{T} = U\mathbb{U}_{\Sigma_\mathbf{T}}U^\top \qquad & \text{(Theorem 1)}. \end{aligned} \tag{50}$$

The reasoning also reverses, so

$$U \text{ is a } \Sigma_\mathbf{T}\text{-minimizer for } \mathbf{T} \iff \mathcal{S}_\mathbf{T} = U\mathbb{U}_{\Sigma_\mathbf{T}}U^\top \tag{51a}$$

$$\iff \mathcal{S}_{\mathbf{A}(\mathbf{T},U)} = \mathbb{U}_{\Sigma_\mathbf{T}}, \tag{51b}$$

the second step being from Eqs. (6) and (24b).

Then from Eqs. (15), (83a), and Theorem 1,

$$U \text{ is a } \Sigma_\mathbf{T}\text{-minimizer for } \mathbf{T} \iff \mathbf{A}(\mathbf{T}, U) \in \boldsymbol{\mathcal{V}}_{\Sigma_\mathbf{T}}(I), \tag{52a}$$

$$\iff [\mathbf{A}(\mathbf{T}, U)]_{\mathbb{BB}} \text{ is a } \Sigma_\mathbf{T} \text{ reference matrix}. \tag{52b}$$

Equation (52b) will eventually tie the notion of $\Sigma_\mathbf{T}$-minimizer to Browaeys & Chevrot [9].

To make $\Sigma_\mathbf{T}$-minimizers more concrete, note, for example, that if U is a $\Sigma_\mathbf{T}$-minimizer for $\mathbf{T}$ and if $\Sigma_\mathbf{T} = \text{ORTH}$, then, from Eq. (51a) and Table 2, the vectors $U\mathbf{i}$, $U\mathbf{j}$, $U\mathbf{k}$—the columns of U—are the 2-fold axes of $\mathbf{T}$. Similarly, if U is a $\Sigma_\mathbf{T}$-minimizer for $\mathbf{T}$ and if $\Sigma_\mathbf{T} = \text{TRIG}$, then the third column of U is the 3-fold axis of $\mathbf{T}$, and the second column is one of the 2-fold axes. And so forth.

9.1 To Find $\Sigma_\mathbf{T}$-Minimizers

From Eq. (11b),

$$V\mathbb{U}_\Sigma V^\top = U\mathbb{U}_\Sigma U^\top \iff U^\top V \in \mathbb{G}_\Sigma \qquad (U, V \in \mathbb{U}). \tag{53}$$

To find a $\Sigma_\mathbf{T}$-minimizer for a given $\mathbf{T}$: Theorem 3 of [54] gives the symmetry group $\mathcal{S}_\mathbf{T}$ in the form $\mathcal{S}_\mathbf{T} = U\mathbb{U}_\Sigma U^\top$, so $\Sigma = \Sigma_\mathbf{T}$ and U is one $\Sigma_\mathbf{T}$-minimizer for $\mathbf{T}$. (See also [8] and [20].) Then from Eqs. (51a) and (53), the set of $\Sigma_\mathbf{T}$-minimizers for $\mathbf{T}$ is

$$U\mathbb{G}_{\Sigma_\mathbf{T}} = \{UG : G \in \mathbb{G}_{\Sigma_\mathbf{T}}\}. \tag{54}$$

Table 3 The high symmetry axes of the groups $U\mathbb{U}_\Sigma U^\top$. See also Table 2.

Group	High symmetry axes	
$U\,\mathbb{U}_{\text{TRIV}}\,U^\top = \{I\}$	All $\mathbf{v} \in \mathbb{S}^2$	(the 1-fold axes)
$U\,\mathbb{U}_{\text{MONO}}\,U^\top$	$\pm U\mathbf{k}$	(the 2-fold axis)
$U\,\mathbb{U}_{\text{ORTH}}\,U^\top$	$\pm U\mathbf{i}$, $\pm U\mathbf{j}$, $\pm U\mathbf{k}$	(the 2-fold axes)
$U\,\mathbb{U}_{\text{TRIG}}\,U^\top$	$\pm U\mathbf{k}$	(the 3-fold axis)
$U\,\mathbb{U}_{\text{TET}}\,U^\top$	$\pm U\mathbf{k}$	(the 4-fold axis)
$U\,\mathbb{U}_{\text{CUBE}}\,U^\top$	$\pm U\mathbf{i}$, $\pm U\mathbf{j}$, $\pm U\mathbf{k}$	(the 4-fold axes)
$U\,\mathbb{U}_{\text{XISO}}\,U^\top$	$\pm U\mathbf{k}$	(the regular axis)
$U\,\mathbb{U}_{\text{ISO}}\,U^\top = \mathbb{U}$	All $\mathbf{v} \in \mathbb{S}^2$	(the regular axes)

9.2 The XISO-Approximation $\mathbf{X}(\mathbf{T}, U)$ when U Is a $\Sigma_\mathbf{T}$-Minimizer

Table 3 gives the high symmetry axes for each elastic symmetry group. They are "high" with respect to the ordering 1-fold, 2-fold, 3-fold, 4-fold, regular.

From Eq. (12), Table 3 can be compactly stated

$$\mathbf{v} \in \mathbb{S}^2 \text{ is a high symmetry axis of } U\mathbb{U}_\Sigma U^\top \iff \mathbf{v} = (UG)\mathbf{k} \text{ for some } G \in \mathbb{G}_\Sigma. \quad (55)$$

Theorem 4 *Let U be a $\Sigma_\mathbf{T}$-minimizer for $\mathbf{T}$. Equivalently, $\mathcal{S}_\mathbf{T} = U\mathbb{U}_{\Sigma_\mathbf{T}}U^\top$. Then*

(i) *The regular axis $U\mathbf{k}$ of the* XISO*-approximation $\mathbf{X}(\mathbf{T}, U)$ is a high symmetry axis of $\mathbf{T}$.*
(ii) *If the regular axis $V\mathbf{k}$ of $\mathbf{X}(\mathbf{T}, V)$ is a high symmetry axis of $\mathbf{T}$, then $V = U'G$ for some $\Sigma_\mathbf{T}$-minimizer U' and some $G \in \mathbb{U}_{\text{XISO}}$.*

Proof From Table 3, $U\mathbf{k}$ is a high symmetry axis of $\mathbf{T}$ (i.e., of $\mathcal{S}_\mathbf{T}$). This proves (i).

Conversely, suppose that the regular axis $V\mathbf{k}$ of $\mathbf{X}(\mathbf{T}, V)$ is a high symmetry axis of $\mathbf{T}$. From Eq. (55), $V\mathbf{k} = (UG')\mathbf{k}$ for some $G' \in \mathbb{G}_{\Sigma_\mathbf{T}}$. Then $(UG')^\top V\,\mathbf{k} = \mathbf{k}$, so $(UG')^\top V \in \mathbb{U}_{\text{XISO}}$, from Table 2. Then $V = (UG')G$ for some $G \in \mathbb{U}_{\text{XISO}}$. Since UG' is a $\Sigma_\mathbf{T}$-minimizer for $\mathbf{T}$, this proves (ii). □

Figure 5 shows XISO-approximations to $\mathbf{T}$ whose regular axes coincide with high symmetry axes of $\mathbf{T}$.

Unless $\mathbf{T}$ is isotropic, the symmetry of $\mathbf{X}(\mathbf{T}, U)$ will normally be XISO, in which case the regular axis of $\mathbf{X}(\mathbf{T}, U)$ is unique. It is possible, however, for the symmetry of $\mathbf{X}(\mathbf{T}, U)$ to be ISO even if $\mathbf{T}$ is not ISO. Then every direction is a regular axis. An example. with $U = I$, is the elastic map $\mathbf{T}$ in Sect. 10.5.

10 Examples of XISO-Approximations

For each point $\mathbf{v} \in \mathbb{S}^2$, we imagine the XISO subspace $\boldsymbol{\mathcal{V}}_{\text{XISO}}(\mathbf{v})$ as being attached to $\mathbb{S}^2$ at $\mathbf{v}$. The subspace consists of all elastic maps having $\mathbf{v}$ as a regular axis; see Fig. 6. For $\mathbf{v} = U\mathbf{k}$, the XISO-approximation $\mathbf{X}(\mathbf{T}, U)$ is in $\boldsymbol{\mathcal{V}}_{\text{XISO}}(\mathbf{v})$ and thus can be regarded as attached to $\mathbb{S}^2$ at $\mathbf{v}$.

Each subspace $\boldsymbol{\mathcal{V}}_{\text{XISO}}(\mathbf{v})$ in principle appears twice on the sphere—at the antipodal points $\mathbf{v}$ and $-\mathbf{v}$. The same is true for any XISO-approximation $\mathbf{X}(\mathbf{T}, U)$. In Figs. 5–12, however,

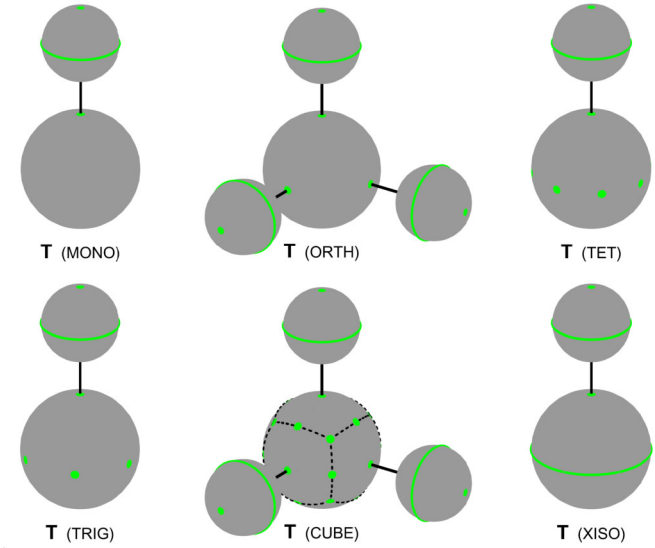

Fig. 5 The XISO-approximations (small spheres) whose regular axis coincides with a high symmetry axis of $\mathbf{T}$. A diagram is shown for each symmetry class $\Sigma \neq$ ISO, TRIV. Symmetry axis locations are shown in green. Only ghost spheres are shown, since $\mathbf{T}$ is not known specifically.

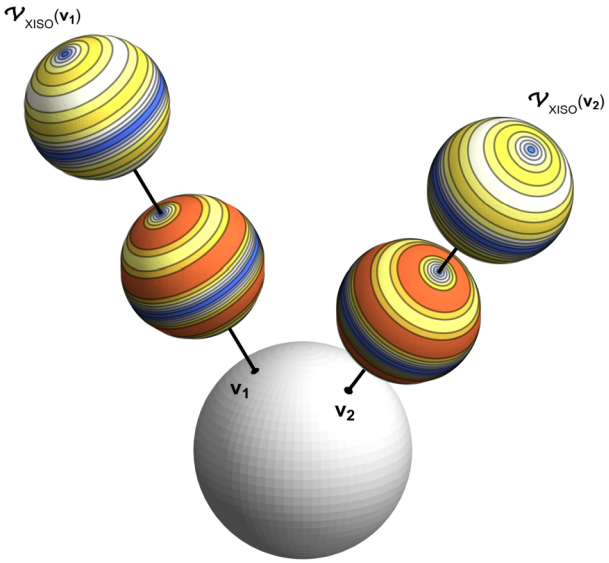

Fig. 6 The set $\mathcal{T}_{\text{XISO}}$, which consists of the elastic maps having a regular axis. To each point $\mathbf{v} \in \mathbb{S}^2$ we imagine attaching all elastic maps that have a regular axis through $\pm\mathbf{v}$; those maps make up the subspace $\mathcal{V}_{\text{XISO}}(\mathbf{v})$. The figure shows only two of the infinitely many elastic maps in $\mathcal{V}_{\text{XISO}}(\mathbf{v})$, and it does so only for $\mathbf{v}_1$ and $\mathbf{v}_2$ rather than for all $\mathbf{v} \in \mathbb{S}^2$. The XISO-approximation $\mathbf{X}(\mathbf{T}, U)$ to an elastic map $\mathbf{T}$ is the projection of $\mathbf{T}$ onto $\mathcal{V}_{\text{XISO}}(\mathbf{v})$, where $\mathbf{v} = U\mathbf{k}$. The closest XISO map to $\mathbf{T}$ is then the closest to $\mathbf{T}$ of all the $\mathbf{X}(\mathbf{T}, U)$, $\mathbf{v} = U\mathbf{k}$, $\mathbf{v} \in \mathbb{S}^2$. Here the white sphere is not meant to depict any elastic map; it is just the unit sphere $\mathbb{S}^2$.

we show each $\mathbf{X}(\mathbf{T}, U)$ only once, at whichever of $\mathbf{v}$ and $-\mathbf{v}$ that is more convenient for depiction.

Figure 6 gives the impression that the subspaces $\mathcal{V}_{\text{XISO}}(\mathbf{v})$ are disjoint. But in fact,

$$\mathbf{v}_1 \neq \pm\mathbf{v}_2 \implies \mathcal{V}_{\text{XISO}}(\mathbf{v}_1) \cap \mathcal{V}_{\text{XISO}}(\mathbf{v}_2) = \mathcal{V}_{\text{ISO}}(I) = \mathcal{T}_{\text{ISO}}. \tag{56}$$

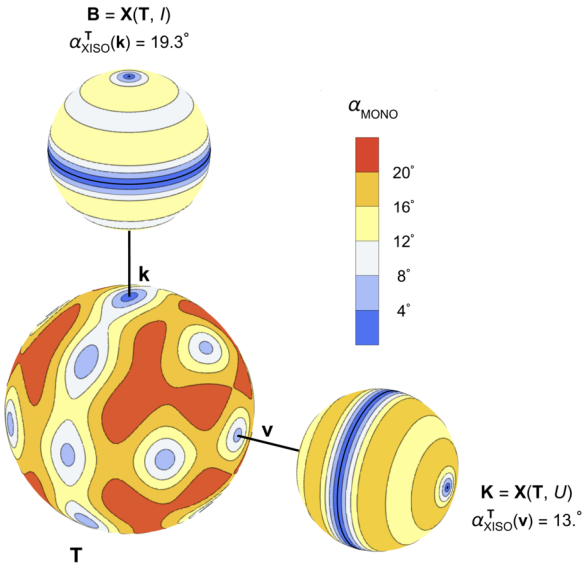

Fig. 7 The monoclinic map **T** of Eq. (57) together with two XISO-approximations **B** and **K** to **T**. The elastic map **B** is the XISO-approximation whose regular axis coincides with the 2-fold axis **k** of **T**. The elastic map **K** is the closest XISO map to **T**. The indicated values $\alpha^{\mathbf{T}}_{\mathrm{XISO}}(\mathbf{k}) = 19.3^\circ$ and $\alpha^{\mathbf{T}}_{\mathrm{XISO}}(\mathbf{v}) = 13^\circ$ show that **K** is a better approximation to **T** than is **B**. This is also seen in the contour plots, though not conspicuously. The color code is the same for all three spheres.

In Sects. 10.1–10.6 we consider various XISO-approximations $\mathbf{X}(\mathbf{T}, U)$. For those labeled with "**B**" or "$\mathbf{B}_i$" in Figs. 7–12, the rotation U is a $\Sigma_{\mathbf{T}}$-minimizer for **T** and, consistent with Theorem 4 and Fig. 5, the regular axis of $\mathbf{X}(\mathbf{T}, U)$ coincides with a high symmetry axis of **T**. For the XISO-approximations labeled with "**K**" or "$\mathbf{K}_i$", the rotation U is an XISO-minimizer and so $\mathbf{X}(\mathbf{T}, U)$ is a closest XISO map to **T**. The elastic maps **T** that we chose are not typical, but they are not impossibly rare either.

10.1 A Monoclinic Example

Let **T** be given by

$$T = [\mathbf{T}]_{\mathbb{BB}} = \begin{pmatrix} 1 & & & & & \\ & 2 & & & & \\ & & 3 & 2 & 1 & \\ & & 2 & 4 & & \\ & & 1 & & 5 & \\ & & & & & 6 \end{pmatrix}. \tag{57}$$

(Blank entries are understood to be zero.)

Since T is a MONO reference matrix, we can shortcut the process of finding $\mathcal{S}_{\mathbf{T}}$ that was mentioned in Sect. 9.1. Since T is a MONO reference matrix, then $\mathcal{S}_{\mathbf{T}} \supset \mathbb{U}_{\mathrm{MONO}}$, by Eq. (82). But in fact $\mathcal{S}_{\mathbf{T}} = \mathbb{U}_{\mathrm{MONO}}$, since the plot of $\alpha^{\mathbf{T}}_{\mathrm{MONO}}$ (Fig. 7) shows that **T** has only two 2-fold points—at $\pm\mathbf{k}$. Thus $\Sigma_{\mathbf{T}} = \mathrm{MONO}$.

Since $\mathcal{S}_{\mathbf{T}} = \mathbb{U}_{\mathrm{MONO}}$, then $U = I$ is a $\Sigma_{\mathbf{T}}$-minimizer for **T**, from Eq. (51a). From Eq. (84b) the matrix of the corresponding XISO-approximation $\mathbf{B} = \mathbf{X}(\mathbf{T}, I)$ is diagonal with entries $3/2, 3/2, 7/2, 7/2, 5, 6$. Consistent with Theorem 4, the regular axis of **B**, namely $I\mathbf{k} = \mathbf{k}$, is also a 2-fold axis of **T**.

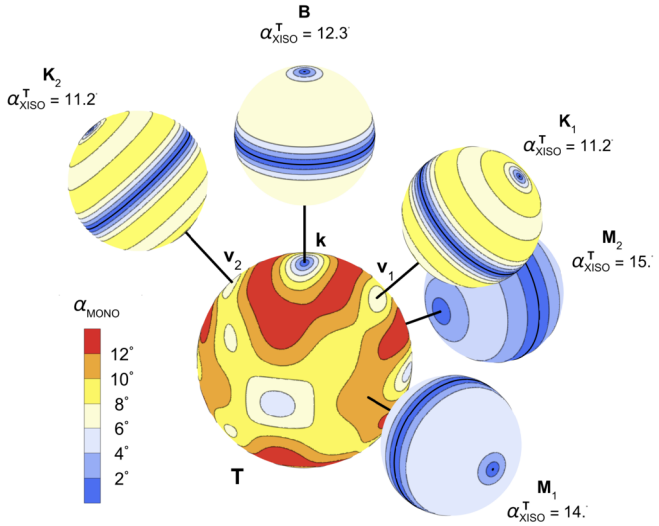

Fig. 8 The monoclinic map $\mathbf{T}$ of Eq. (59) and five XISO-approximations to it. The elastic map $\mathbf{B}$ is the XISO-approximation whose regular axis is the 2-fold axis $\mathbf{k}$ of $\mathbf{T}$. The elastic maps $\mathbf{K}_1$ and $\mathbf{K}_2$ are the closest XISO maps to $\mathbf{T}$. See Eq. (61) for $\mathbf{M}_1$ and $\mathbf{M}_2$. The values of $\alpha^{\mathbf{T}}_{\text{XISO}}$ show that $\mathbf{K}_1$ and $\mathbf{K}_2$ are somewhat better approximations to $\mathbf{T}$ than is $\mathbf{B}$, and that they are much better approximations than are $\mathbf{M}_1$ and $\mathbf{M}_2$. This is also seen in the contour plots.

An XISO-minimizer for $\mathbf{T}$ can be calculated from Eq. (46). One such is

$$U = \begin{pmatrix} 0 & -0.940 & 0.342 \\ 0 & 0.342 & 0.940 \\ -1 & 0 & 0 \end{pmatrix}, \tag{58}$$

but any rotation matrix whose third column is plus or minus the third column of U is also an XISO-minimizer. The closest XISO map $\mathbf{K} = \mathbf{X}(\mathbf{T}, U)$ to $\mathbf{T}$ is then calculated from Eqs. (31a), (31b) and (84b). Its regular axis is $\mathbf{v} = U\mathbf{k} = (0.342,\ 0.940,\ 0)$.

The main points here are that $\mathbf{B}$ and $\mathbf{K}$ are not the same, and that $\mathbf{B}$—the XISO-approximation whose regular axis coincides with the 2-fold axis of $\mathbf{T}$—is not the best approximation to $\mathbf{T}$.

10.2 Another Monoclinic Example

The elastic map $\mathbf{T}$ is defined by

$$[\mathbf{T}]_{\mathbb{BB}} = \begin{pmatrix} 28 & -2 & & & & & \\ -2 & 61 & & & & & \\ & & 71 & -4 & 6 & 8 \\ & & -4 & 68 & 10 & \\ & & 6 & 10 & 62 & -3 \\ & & 8 & & -3 & 59 \end{pmatrix}. \tag{59}$$

As in Sect. 10.1, the symmetry group $\mathcal{S}_{\mathbf{T}}$ of $\mathbf{T}$ is found to be $\mathbb{U}_{\text{MONO}}$, and $U = I$ is then a $\Sigma_{\mathbf{T}}$-minimizer for $\mathbf{T}$. The corresponding XISO-approximation $\mathbf{B} = \mathbf{X}(\mathbf{T}, I)$ is found imme-

diately from Eq. (84b). Consistent with Theorem 4, its regular axis $I\mathbf{k} = \mathbf{k}$ is a 2-fold axis of $\mathbf{T}$.

From Eq. (46), an XISO-minimizer U_1 for $\mathbf{T}$ is

$$U_1 = \begin{pmatrix} 0.118 & -0.986 & 0.114 \\ 0.708 & 0.164 & 0.687 \\ -0.697 & 0 & 0.718 \end{pmatrix}. \tag{60}$$

The matrix of the corresponding closest map $\mathbf{K}_1 = \mathbf{X}(\mathbf{T}, U_1)$ to $\mathbf{T}$ is found from Eqs. (31a), (31b), and (84b). Its regular axis—the third column of U_1—is $\mathbf{v}_1 = (0.11, 0.69, 0.72)$. Since $\mathbf{K}_1$ does not have Z_π as a symmetry, another closest XISO map $\mathbf{K}_2$ is inevitable, with regular axis $\mathbf{v}_2 = Z_\pi \mathbf{v}_1$.

Figure 8 shows $\mathbf{B}$, $\mathbf{K}_1$, $\mathbf{K}_2$, as well as the XISO-approximations $\mathbf{M}_1 = \mathbf{X}(\mathbf{T}, M_1)$ and $\mathbf{M}_2 = \mathbf{X}(\mathbf{T}, M_2)$, where

$$M_1 = \begin{pmatrix} 0.658 & 0 & 0.753 \\ -0.753 & 0 & 0.658 \\ 0 & -1 & 0 \end{pmatrix}, \quad M_2 = \begin{pmatrix} -0.707 & 0 & -0.707 \\ -0.707 & 0 & 0.707 \\ 0 & 1 & 0 \end{pmatrix}. \tag{61}$$

We calculated M_1 and M_2 using the routine `MS_axes.m` [57], which is supposed to implement Browaeys & Chevrot [9]. The rotation M_2 was calculated with their `X3_stiff` option, M_1 without it.

In each of Figs. 7–12, the $\alpha^{\mathbf{T}}_{\text{XISO}}$ values are consistent with the contour plot for $\mathbf{T}$. Here in Fig. 8, for example, we imagine a band consisting of points on the large sphere that are within, say, 5° of the great circle with poles at $\pm\mathbf{v}_1$. The colors on that band—mostly yellow or cooler—are cooler than the colors on the comparable band at the equator (blue = cold, red = hot). Thus $\mathbf{T}$ looks more like an elastic map with regular axis $\mathbf{v}_1$ than an elastic map with regular axis $\mathbf{k}$.

10.3 An Orthorhombic Example

The elastic map $\mathbf{T}$ is defined by

$$T = [\mathbf{T}]_{\mathbb{BB}} = \begin{pmatrix} 86 & & & & & \\ & 51 & & & & \\ & & 32 & & & \\ & & & 46 & -20 & 13 \\ & & & -20 & 45 & -2 \\ & & & 13 & -2 & 87 \end{pmatrix}. \tag{62}$$

Since T is an ORTH reference matrix then $\mathcal{S}_{\mathbf{T}} \supset \mathbb{U}_{\text{ORTH}}$, by Eq. (82). But in fact $\mathcal{S}_{\mathbf{T}} = \mathbb{U}_{\text{ORTH}}$, since $\mathbf{T}$ has six distinct eigenvalues—too many for it to be tetragonal. Hence $\Sigma_{\mathbf{T}} = \text{ORTH}$.

Since $\mathcal{S}_{\mathbf{T}} = \mathbb{U}_{\text{ORTH}}$, the identity rotation I is one $\Sigma_{\mathbf{T}}$-minimizer for $\mathbf{T}$, from Eq. (51a). From Eq. (54), two others are then $U_{\mathbf{i}}$ and $U_{\mathbf{j}}$. ($U_{\mathbf{v}}$ is defined in Eq. (23).) The corresponding XISO-approximations $\mathbf{B}_3 = \mathbf{X}(\mathbf{T}, I)$, $\mathbf{B}_1 = \mathbf{X}(\mathbf{T}, U_{\mathbf{i}})$, $\mathbf{B}_2 = \mathbf{X}(\mathbf{T}, U_{\mathbf{j}})$ are calculated from Eqs. (84b), (31a) and (31b). Consistent with Theorem 4, their regular axes are 2-fold axes of $\mathbf{T}$; see Fig. 9.

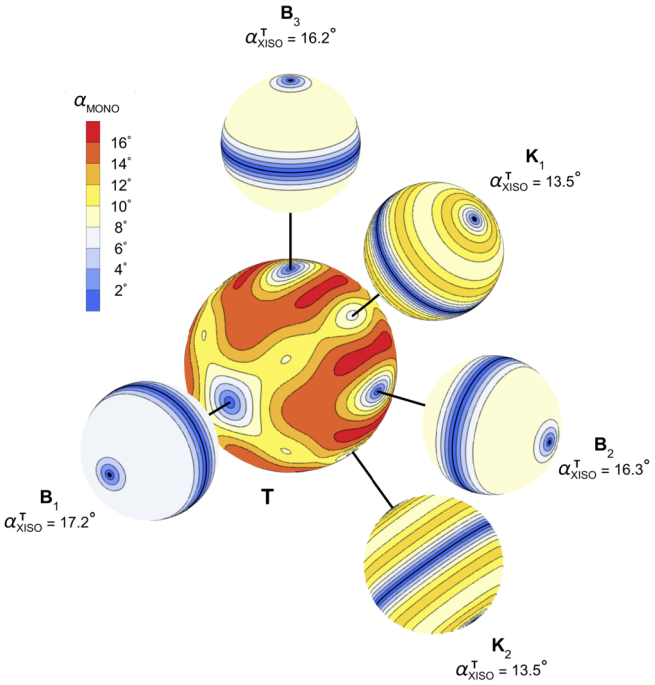

Fig. 9 The orthorhombic elastic map **T** of Eq. (62) and five XISO-approximations to it. The elastic maps $\mathbf{B}_1$, $\mathbf{B}_2$, $\mathbf{B}_3$ are the XISO-approximations whose regular axis is a 2-fold axis of **T**, and $\mathbf{K}_1$ and $\mathbf{K}_2$ are the closest XISO maps to **T**. The values of $\alpha^{\mathbf{T}}_{\mathrm{XISO}}$ in the figure show that $\mathbf{K}_1$ and $\mathbf{K}_2$ are better approximation to **T** than are $\mathbf{B}_1$, $\mathbf{B}_2$, or $\mathbf{B}_3$. This is also seen in the contour plots

From Eq. (46), an XISO-minimizer U_1 for **T** is

$$U_1 = \begin{pmatrix} 0 & -1 & 0 \\ 0.7041 & 0 & 0.7101 \\ -0.7101 & 0 & 0.7041 \end{pmatrix}. \tag{63}$$

The matrix of the corresponding closest XISO map $\mathbf{K}_1$ to **T** is then, from Eqs. (31a), (31b), and (84b),

$$[\mathbf{K}_1] = [\mathbf{X}(\mathbf{T}, U_1)] = \begin{pmatrix} 73.95 & & & 9.53 & -5.11 & 5.34 \\ & 45.04 & -10.28 & & & \\ & -10.28 & 44.86 & & & \\ 9.53 & & & 54.85 & -11.55 & 2.69 \\ -5.11 & & & -11.55 & 41.30 & -1.50 \\ 5.34 & & & 2.69 & -1.50 & 87.00 \end{pmatrix}, \tag{64}$$

Its regular axis—the third column of U_1—is $\mathbf{v}_1 = (0, 0.7101, 0.7041)$. The other closest XISO map $\mathbf{K}_2$ then has regular axis $\mathbf{v}_2 = Z_\pi \mathbf{v}_1$.

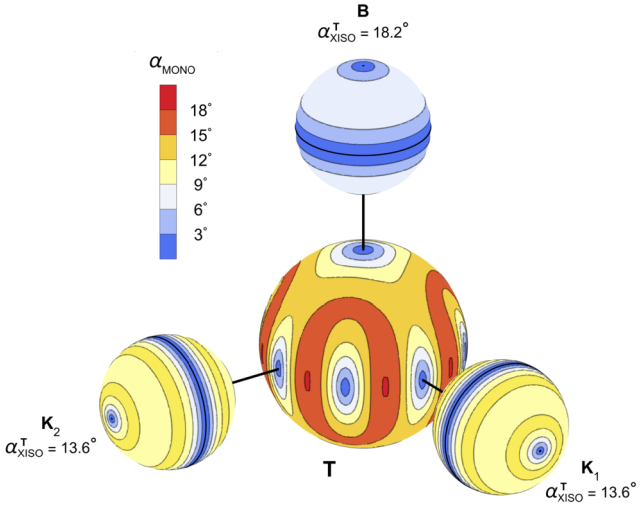

Fig. 10 The tetragonal elastic map $\mathbf{T}$ of Eq. (65) and three XISO-approximations to it. The elastic map $\mathbf{B}$ is the XISO-approximation whose regular axis is the 4-fold axis of $\mathbf{T}$, and $\mathbf{K}_1$ and $\mathbf{K}_2$ are the closest XISO maps to $\mathbf{T}$. The values of $\alpha^{\mathbf{T}}_{\mathrm{XISO}}$ show that $\mathbf{K}_1$ and $\mathbf{K}_2$ are better approximation to $\mathbf{T}$ than is $\mathbf{B}$. This is also seen in the contour plots

10.4 A Tetragonal Example

The elastic map $\mathbf{T}$ is defined by

$$T = [\mathbf{T}]_{\mathbb{BB}} = \begin{pmatrix} 60 & & & & & & \\ & 60 & & & & & \\ & & 15 & & & & \\ & & & 71 & & & \\ & & & & 58 & 6 & \\ & & & & 6 & 15 & \end{pmatrix}. \tag{65}$$

Since T is a TET reference matrix then $\mathcal{S}_{\mathbf{T}} \supset \mathbb{U}_{\mathrm{TET}}$. But since $\mathbf{T}$ has five distinct eigenvalues—too many for it to be cubic or transverse isotropic, then in fact $\mathcal{S}_{\mathbf{T}} = \mathbb{U}_{\mathrm{TET}}$. (Or if the plot for $\mathbf{T}$ is available, as in Fig. 10, just note that the plot does not have CUBE or XISO symmetry.) Hence $\Sigma_{\mathbf{T}} = \mathrm{TET}$.

Since $\mathcal{S}_{\mathbf{T}} = \mathbb{U}_{\mathrm{TET}}$, the rotation $U = I$ is a $\Sigma_{\mathbf{T}}$-minimizer for $\mathbf{T}$. The corresponding XISO-approximation $\mathbf{B} = \mathbf{X}(\mathbf{T}, I)$ is easily calculated from Eq. (84b). Consistent with Theorem 4, its regular axis is the 4-fold axis $\mathbf{k}$ of $\mathbf{T}$.

From Eq. (46), an XISO-minimizer U_1 for $\mathbf{T}$ is

$$U_1 = \frac{1}{\sqrt{2}} \begin{pmatrix} 0 & -1 & 1 \\ 0 & 1 & 1 \\ -\sqrt{2} & 0 & 0 \end{pmatrix}. \tag{66}$$

The matrix of the corresponding closest XISO map $\mathbf{K}_1$ to $\mathbf{T}$ is found from Eqs. (31a), (31b), and (84b). Its regular axis is $\mathbf{v}_1 = U_1\mathbf{k} = 1\ 1\ 0$. The other closest XISO map $\mathbf{K}_2$ then has regular axis $\mathbf{v}_2 = Z_{\pi/2}\mathbf{v}_1$.

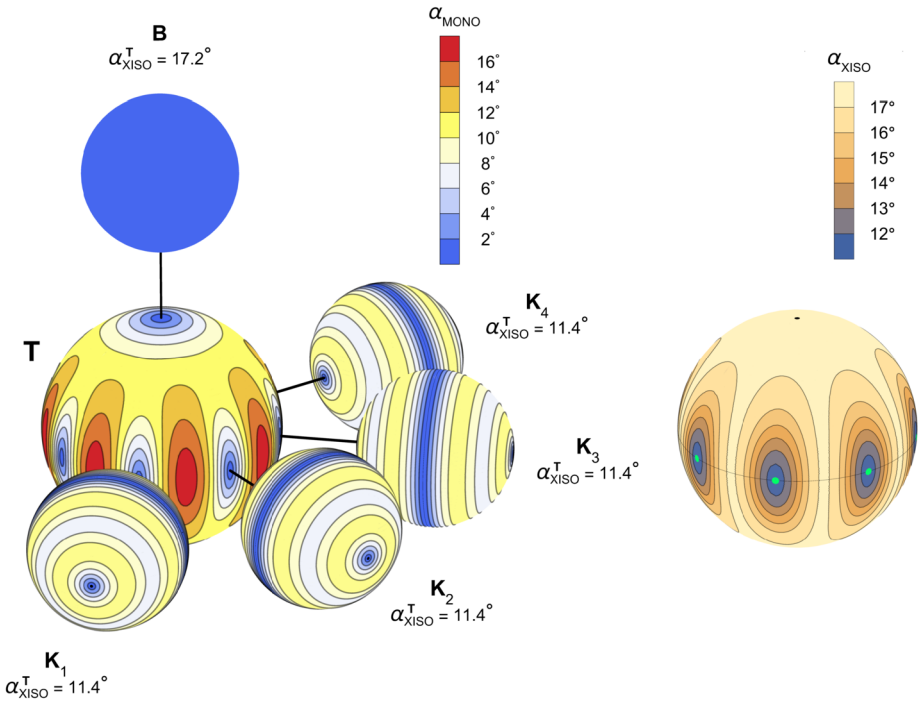

Fig. 11 (*Left*) The tetragonal elastic map $\mathbf{T}$ of Eq. (67) and five XISO-approximations to it, all depicted as contour plots of their MONO angle functions as usual. The elastic map $\mathbf{B}$ is the XISO-approximation with a regular axis coinciding with the 4-fold axis of $\mathbf{T}$, and $\mathbf{K}_1, \mathbf{K}_2, \mathbf{K}_3, \mathbf{K}_4$ are closest XISO maps to $\mathbf{T}$. The values of $\alpha^{\mathbf{T}}_{\text{XISO}}$ show that $\mathbf{K}_1, \mathbf{K}_2, \mathbf{K}_3, \mathbf{K}_4$ are much better approximations to $\mathbf{T}$ than is $\mathbf{B}$. (*Right*) Contour plot of $\alpha^{\mathbf{T}}_{\text{XISO}}$. The minima of $\alpha^{\mathbf{T}}_{\text{XISO}}$ (green points) are at the regular axes of $\mathbf{K}_1, \mathbf{K}_2, \mathbf{K}_3, \mathbf{K}_4$

10.5 Another Tetragonal Example

The elastic map $\mathbf{T}$ is defined by

$$T = [\mathbf{T}]_{\mathbb{BB}} = \begin{pmatrix} 2 & & & & & \\ & 2 & & & & \\ & & 3 & & & \\ & & & 1 & & \\ & & & & 2 & \\ & & & & & 1 \end{pmatrix}. \tag{67}$$

Since T is a TET reference matrix then $\mathcal{S}_{\mathbf{T}} \supset \mathbb{U}_{\text{TET}}$. But since the plot for $\mathbf{T}$ in Fig. 11 does not have CUBE or XISO symmetry, then in fact $\mathcal{S}_{\mathbf{T}} = \mathbb{U}_{\text{TET}}$. Hence $\Sigma_{\mathbf{T}} = \text{TET}$.

Since $\mathcal{S}_{\mathbf{T}} = \mathbb{U}_{\text{TET}}$, the rotation $U = I$ is a $\Sigma_{\mathbf{T}}$-minimizer for $\mathbf{T}$. From Eq. (84b) the matrix of the corresponding XISO-approximation $\mathbf{B} = \mathbf{X}(\mathbf{T}, I)$ is diagonal with diagonal entries 2, 2, 2, 2, 2, 1—it is isotropic.

Here the elastic map $\mathbf{T}$ is simple enough that its XISO-minimizers can be found analytically, without resorting to the numerical algorithm mentioned in Sect. 8.1. The function g to be minimized is, from Eqs. (49), (48), (33),

$$g(\theta, \sigma, \phi) = d\big(\mathbf{T}, \boldsymbol{\nu}_{\text{XISO}}(\widehat{U}_{(\theta,\sigma,\phi)})\big)$$

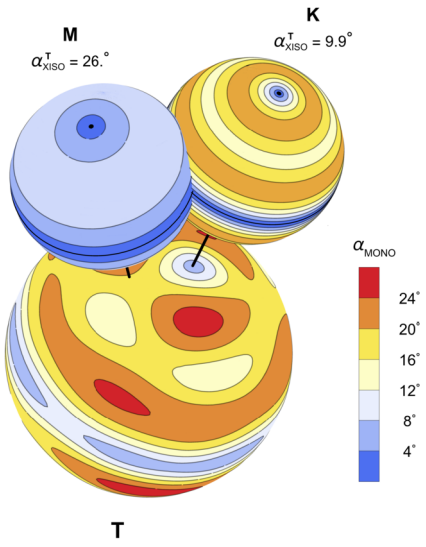

Fig. 12 The same elastic map **T** and XISO-approximations from Figs. 3 and 4. The elastic map **K** is $\mathbf{T}'$ from Fig. 4 and is the closest XISO map to **T**, and **M** is $\mathbf{T}'$ from Fig. 3 and is the XISO-approximation to **T** computed using [57]. The values of $\alpha^{\mathbf{T}}_{\text{XISO}}$ show that **K** is a better approximation to **T** than is **M**. This is also seen in the contour plots

$$= \frac{1}{64}\sqrt{a_1 + a_2\cos 2\phi - a_3\cos 4\phi + a_4\cos 6\phi - a_5\cos 8\phi - a_6\cos 8\theta\sin^8\phi},$$

$$a_1 = \frac{15159}{2},\ a_2 = 980,\ a_3 = 490,\ a_4 = 140,\ a_5 = \frac{35}{2},\ a_6 = 2240, \tag{68}$$

independent of σ, as expected from Theorem 2. The global minima of g are at $(\theta, \sigma, \phi) = (n\pi/4,\ \sigma,\ \pi/2)$ with value $g = \sqrt{29/32}$. The XISO-minimizers for **T** are therefore, for any σ and any integral n,

$$\widehat{U}_{(n\pi/4,\,\sigma,\,\pi/2)} = \begin{pmatrix} -\sin t\,\sin\sigma & -\sin t\,\cos\sigma & \cos t \\ \cos t\,\sin\sigma & \cos t\,\cos\sigma & \sin t \\ -\cos\sigma & \sin\sigma & 0 \end{pmatrix} \quad (t = n\pi/4). \tag{69}$$

Although there are infinitely many XISO-minimizers, they have only eight distinct third columns. They give the regular axes of the closest XISO-maps to **T** (the green points in Fig. 11). The closest XISO-maps themselves are

$$\mathbf{K}_n = \mathbf{X}\big(\mathbf{T},\ \widehat{U}_{(n\pi/4,\,\sigma,\,\pi/2)}\big) \quad (n = 1, 2, 3, 4). \tag{70}$$

They are computed from Eqs. (43), (31a), (31b), (84b).

The elastic map **T**, like the map mentioned in footnote (2), has the peculiar property that $\alpha^{\mathbf{T}}_{\text{MONO}}$ has more symmetry than does **T** itself. Here $\alpha^{\mathbf{T}}_{\text{MONO}}$ has all the elements of D_8 as symmetries. To show this analytically, one need only verify that $Z_{\pi/4}$ is a symmetry of $\alpha^{\mathbf{T}}_{\text{MONO}}$. Since X_π is a symmetry of **T** and hence is a symmetry of $\alpha^{\mathbf{T}}_{\text{MONO}}$, and since $Z_{\pi/4}$ and X_π generate D_8, then indeed all 16 members of D_8 are symmetries of $\alpha^{\mathbf{T}}_{\text{MONO}}$.

10.6 The Trivial Elastic Map T from Figs. 3 and 4

Figure 12 shows **T** and the two XISO-approximations to it from Figs. 3 and 4. As before, **T** is from Eq. (93). From the contour plot of $\alpha^{\mathbf{T}}_{\text{MONO}}$ in Fig. 12, whose coolest color is light

blue, $\mathbf{T}$ has no 2-fold points. Hence $\Sigma_{\mathbf{T}} = \text{TRIV}$. (Or one can compute from Eq. (45) that $d(\mathbf{T}, \mathcal{T}_{\text{MONO}}) > 0$.)

The XISO-approximations $\mathbf{M}$ and $\mathbf{K}$ are $\mathbf{T}'$ from Figs. 3 and 4 respectively. Again we see that $\mathbf{M}$ fails as an approximation to $\mathbf{T}$.

For any trivial elastic map $\mathbf{T}$, every $U \in \mathbb{U}$ is a $\Sigma_{\mathbf{T}}$-minimizer, since $U\mathbb{U}_{\text{TRIV}}U^{\top} = \mathbb{U}_{\text{TRIV}}$. Thus, whereas restricting U to be a $\Sigma_{\mathbf{T}}$-minimizer in Fig. 9 resulted in the three XISO-approximations $\mathbf{B}_1$, $\mathbf{B}_2$, $\mathbf{B}_3$, doing the same in Fig. 12 would give infinitely many XISO-approximations. There would be a small sphere attached to every point of the large sphere.

10.7 A Sufficient Condition for Multiple Closest Σ-Maps

As in Sect. 8, an elastic map $\mathbf{K}$ is a closest Σ-map to an elastic map $\mathbf{T}$ when

$$\mathbf{K} \in \mathcal{T}_{\Sigma}, \quad d(\mathbf{T}, \mathbf{K}) = d(\mathbf{T}, \mathcal{T}_{\Sigma}). \tag{71}$$

As in Figs. 8–11, some elastic maps have more than one closest Σ-map. One way this can happen is if $\mathbf{K}$ is a closest Σ-map to $\mathbf{T}$ and if $V \in \mathbb{U}$ is a symmetry of $\mathbf{T}$ but not a symmetry of $\mathbf{K}$. Then

$$\begin{aligned} d(\mathbf{T}, \mathcal{T}_{\Sigma}) &= d(\mathbf{T}, \mathbf{K}) \\ &= d(\overline{V} \circ \mathbf{T} \circ \overline{V}^{*}, \ \overline{V} \circ \mathbf{K} \circ \overline{V}^{*}) \\ &= d(\mathbf{T}, \underbrace{\overline{V} \circ \mathbf{K} \circ \overline{V}^{*}}_{\neq \mathbf{K}}). \end{aligned} \tag{72}$$

Thus $\overline{V} \circ \mathbf{K} \circ \overline{V}^{*}$ is another closest Σ-map to $\mathbf{T}$.

The closest XISO-maps $\mathbf{K}_1$ and $\mathbf{K}_2$ to $\mathbf{T}$ in Fig. 8 fit the above paradigm. That is, $\mathbf{K}_1$ was a closest XISO-map to $\mathbf{T}$, and $V = Z_{\pi}$ was a symmetry of $\mathbf{T}$ but not a symmetry of $\mathbf{K}_1$. And $\mathbf{K}_2 = \overline{V} \circ \mathbf{K} \circ \overline{V}^{*}$. Figures 9 and 10 are similar.

In Fig. 11 the closest XISO maps $\mathbf{K}_1$ and $\mathbf{K}_3$ fit the paradigm (with $V = Z_{\pi/2}$), as do $\mathbf{K}_2$ and $\mathbf{K}_4$, but $\mathbf{K}_1$ and $\mathbf{K}_2$, for example, do not fit. (The rotation $Z_{\pi/4}$ is not a symmetry of $\mathbf{T}$.)

The 4-fold members of a cubic elastic symmetry group have their axes in three independent directions. The only two 4-fold members of an XISO-group have a common axis—the regular axis. Thus the cubic group cannot be a subgroup of the XISO-group. If $\mathbf{K}$ is a closest XISO-map to a cubic map $\mathbf{T}$, then there must be a symmetry V of $\mathbf{T}$ that is not a symmetry[4] of $\mathbf{K}$. Every cubic map therefore has multiple closest XISO-maps to it. In a thoughtful paper in 2005, Dellinger [18] already anticipated this result with an example.

11 Lattice of Closest Σ Maps

For $\mathbf{T}$ as in Eq. (93), and for each $\Sigma = \text{ISO}, \ldots, \text{TRIV}$, Fig. 13 shows the contour plot of the monoclinic angle function of a closest Σ-map $\mathbf{K}_{\Sigma}$ to $\mathbf{T}$. The various $\mathbf{K}_{\Sigma}$ give some perspective on $\mathbf{K}_{\text{XISO}}$ and indeed offer alternatives to $\mathbf{K}_{\text{XISO}}$. The number β_{Σ} is the angle between $\mathbf{T}$ and $\mathbf{K}_{\Sigma}$. The dashed lines in the figure indicate inclusions among the $\mathcal{T}_{\Sigma}$; the line from the TRIG node to the CUBE node, for example, means that $\mathcal{T}_{\text{CUBE}} \subset \mathcal{T}_{\text{TRIG}}$. As a result, the angles β_{Σ} increase (or are unchanged) going upwards along dashed lines.

[4] We are using the fact that a closest member of $\mathcal{T}_{\text{XISO}}$ to an elastic map $\mathbf{T}$ cannot be isotropic unless $\mathbf{T}$ itself is isotropic.

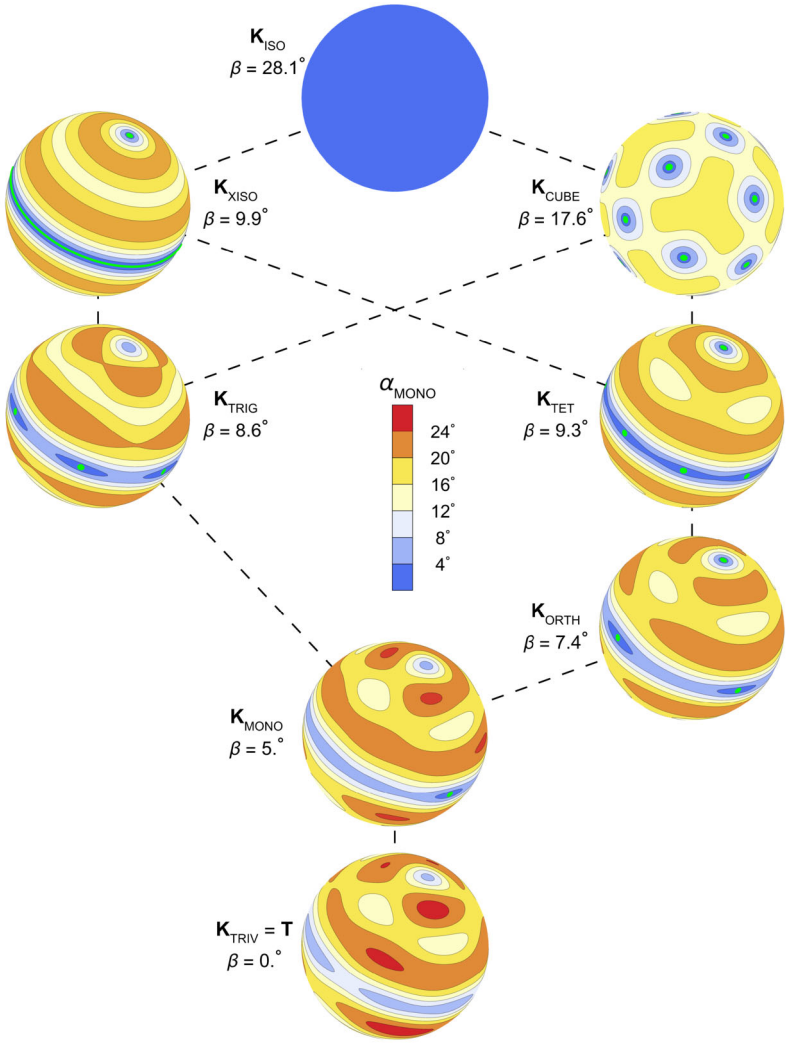

Fig. 13 A closest Σ-map $\mathbf{K}_\Sigma$ to $\mathbf{T}$ for each symmetry class Σ. The number $\beta = \beta_\Sigma$ is the angle between $\mathbf{T}$ and $\mathbf{K}_\Sigma$. To make the 2-fold points of $\mathbf{K}_\Sigma$ conspicuous, they are shown in green; if colored consistently with the color code, they would have been dark blue, since their α_{MONO} values are zero. No 2-fold points, however, are shown on the isotropic sphere; had they been shown, the entire sphere would have been green. The given elastic map $\mathbf{T}$, at bottom, is the same as in Figs. 3 and 4.

12 The Σ-Percentages

For an elastic map $\mathbf{T}$, the notion of the percentage of it with specified symmetry Σ is central to Browaeys & Chevrot [9], but we do not find a definition of it in their paper. The closest we come is their hint that [9, Sect. 4.1.1]

The different elastic symmetry parts of the tensor are presented as percentages of the norm of the elastic tensor in the histogram of Fig. 1 using the following convention:

$$100 \text{ per cent } =$$
$$N^{-2}(\mathbf{X})\big[N^2(\mathbf{X}_{\text{tric}}) + N^2(\mathbf{X}_{\text{mon}}) + N^2(\mathbf{X}_{\text{ort}}) + N^2(\mathbf{X}_{\text{tet}}) + N^2(\mathbf{X}_{\text{hex}}) + N^2(\mathbf{X}_{\text{iso}})\big].$$

That suggests that they were defining the Σ-percentage of $\mathbf{T}$ to be

$$q_\Sigma(\mathbf{T}, U) = \frac{\|\mathbf{Q}_\Sigma(\mathbf{T}, U)\|^2}{\|\mathbf{T}\|^2}. \tag{73}$$

That is what Beller & Chevrot [6] do; our Eq. (73), with $U = I$, will reproduce the six Σ-percentages in their Appendix B. The equation does not, however, reproduce the percentages given in Browaeys & Chevrot [9, Sections 4.1.1, 4.1.2]. Instead, they [9] seem to be calculating the percentage as

$$p_{\Sigma_k}(\mathbf{T}, U) = \frac{\big\|\mathbf{T} - \mathbf{P}\big(\mathbf{T},\, \boldsymbol{\mathcal{V}}_{\Sigma_{k-1}}(U)\big)\big\| - \big\|\mathbf{T} - \mathbf{P}\big(\mathbf{T},\, \boldsymbol{\mathcal{V}}_{\Sigma_k}(U)\big)\big\|}{\|\mathbf{T}\|}. \tag{74a}$$

Equivalently,

$$p_{\Sigma_k}(\mathbf{T}, U) = d\big(\widehat{\mathbf{T}},\, \boldsymbol{\mathcal{V}}_{\Sigma_{k-1}}(U)\big) - d\big(\widehat{\mathbf{T}},\, \boldsymbol{\mathcal{V}}_{\Sigma_k}(U)\big) \qquad \big(\widehat{\mathbf{T}} = \mathbf{T}/\|\mathbf{T}\|\big). \tag{74b}$$

Equation (74a) follows from [59] using our Eq. (38). And $p_\Sigma(\mathbf{T}, U)$, with $U = I$, does match the Browaeys and Chevrot percentages in their Sects. 4.1.1 and 4.1.2.

For a given $\mathbf{T}$ and U the six numbers $q_{\Sigma_k}(\mathbf{T}, U)$ sum to 1, since the summands are pairwise orthogonal (as follows from Eq. (37b)). The numbers $p_{\Sigma_k}(\mathbf{T}, U)$ likewise sum to 1:

$$\sum_{k=1}^{6} p_{\Sigma_k}(\mathbf{T}, U) = d\big(\widehat{\mathbf{T}}, \boldsymbol{\mathcal{V}}_{\Sigma_0}(U)\big) - d\big(\widehat{\mathbf{T}}, \boldsymbol{\mathcal{V}}_{\Sigma_6}(U)\big) = \big\|\widehat{\mathbf{T}}\big\| - 0 = 1. \tag{75}$$

Equation (73), defining the Σ-percentage as $q_\Sigma(\mathbf{T}, U)$, has the virtue that it is transparent. Equations (74a) and (74b), defining the Σ-percentage as $p_\Sigma(\mathbf{T}, U)$, are on the other hand opaque (to us). In no way do they express an intuition for Σ-percentage, whatever that is. Equation (73) has its own seemingly fatal flaw, in that the summands $\mathbf{Q}_\Sigma(\mathbf{T}, U)$, with the exception of $\mathbf{Q}_{\text{ISO}}(\mathbf{T}, U)$, are never physically permissible (Sect. 12.3). Both $q_\Sigma(\mathbf{T}, U)$ and $p_\Sigma(\mathbf{T}, U)$ have the additional complication that they depend on the rotation matrix U.

Although we think neither $q_\Sigma(\mathbf{T}, U)$ nor $p_\Sigma(\mathbf{T}, U)$ is a viable expression of Σ-percentage, we consider $p_\Sigma(\mathbf{T}, U)$ further in the next sections, mainly to clarify the role (and difficulties) of U.

12.1 Calculating the Percentages

From Eqs. (74a) and (33),

$$p_{\Sigma_k}(\mathbf{T}, U) = \frac{\big\|A - P\left(A,\, \mathcal{V}^{\mathbb{B}}_{\Sigma_{k-1}}(I)\right)\big\| - \big\|A - P\left(A,\, \mathcal{V}^{\mathbb{B}}_{\Sigma_k}(I)\right)\big\|}{\|A\|}. \tag{76}$$

The percentage $p_\Sigma(\mathbf{T}, U)$ can now be calculated from Eqs. (76), (31b), (32), (84a)–(84h).

12.2 Sample Calculation of Percentages $p_{\mathbf{\Sigma}}(\mathbf{T}, U)$

We let $\mathbf{T}$ be the elastic map whose matrix with respect to $\mathbb{B}$ is

$$T = \begin{pmatrix} 1 & & & & & \\ & 2 & & & & \\ & & 5 & & & \\ & & & 1 & & \\ & & & & 1 & \\ & & & & & 1 \end{pmatrix}. \tag{77a}$$

$\mathbf{T}$ is orthorhombic, since T is an ORTH-reference matrix, and since the distance $d(\mathbf{T}, \boldsymbol{\mathcal{T}}_{\text{TET}})$ is found to be non-zero, so that $\mathbf{T}$ is not tetragonal. For U we take I, $U_{\mathbf{i}}$, $U_{\mathbf{j}}$ as examples. From Eq. (23), they are

$$I = \begin{pmatrix} 1 & & \\ & 1 & \\ & & 1 \end{pmatrix}, \quad U_{\mathbf{i}} = \begin{pmatrix} & & 1 \\ & -1 & \\ 1 & & \end{pmatrix} = 1\,0\,1_2, \quad U_{\mathbf{j}} = \begin{pmatrix} -1 & & \\ & & 1 \\ & 1 & \end{pmatrix} = 0\,1\,1_2 \tag{77b}$$

From Eq. (32),

$$\begin{aligned} [\overline{I}]_{\mathbb{BB}} &= I_{6\times 6}, \\ [\overline{U_{\mathbf{i}}}]_{\mathbb{BB}} &= \frac{1}{2}\begin{pmatrix} & & -2 & & & \\ & 2 & & & & \\ -2 & & & & & \\ & & & 1 & \sqrt{3} & \\ & & & \sqrt{3} & -1 & \\ & & & & & 2 \end{pmatrix}, \\ [\overline{U_{\mathbf{j}}}]_{\mathbb{BB}} &= \frac{1}{2}\begin{pmatrix} 2 & & & & & \\ & & -2 & & & \\ & -2 & & & & \\ & & & 1 & -\sqrt{3} & \\ & & & -\sqrt{3} & -1 & \\ & & & & & 2 \end{pmatrix}, \end{aligned} \tag{77c}$$

Eqs. (77a) and (31b) then give $A(T, I) = T$ and

$$A(T, U_{\mathbf{i}}) = \begin{pmatrix} 5 & & & & & \\ & 2 & & & & \\ & & 1 & & & \\ & & & 1 & & \\ & & & & 1 & \\ & & & & & 1 \end{pmatrix}, \quad A(T, U_{\mathbf{j}}) = \begin{pmatrix} 1 & & & & & \\ & 5 & & & & \\ & & 2 & & & \\ & & & 1 & & \\ & & & & 1 & \\ & & & & & 1 \end{pmatrix}. \tag{77d}$$

The percentages $p_{\Sigma}(\mathbf{T}, U)$ are then, from Eq. (76),

U	$p_{\text{ISO}}(\mathbf{T}, U)$	$p_{\text{XISO}}(\mathbf{T}, U)$	$p_{\text{TET}}(\mathbf{T}, U)$	$p_{\text{ORTH}}(\mathbf{T}, U)$	$p_{\text{MONO}}(\mathbf{T}, U)$	$p_{\text{TRIV}}(\mathbf{T}, U)$
I	0.4	0.10	0.38	0.12	0	0
$U_{\mathbf{i}}$	0.4	0.23	0.00	0.37	0	0
$U_{\mathbf{j}}$	0.4	0.10	0.02	0.49	0	0

(77e)

12.3 The Summands and the Percentages q_Σ Have No Physical Meaning

From Eqs. (35) and (87), the trace of the summand $\mathbf{Q}_{\Sigma_k}(\mathbf{T}, U)$ is zero unless $k = 1$:

$$\begin{aligned}\operatorname{tr}\left(\mathbf{Q}_{\Sigma_k}(\mathbf{T}, U)\right) &= \operatorname{tr}\left(\mathbf{P}\left(\mathbf{T},\ \boldsymbol{\mathcal{V}}_{\Sigma_k}(U)\right)\right) - \operatorname{tr}\left(\mathbf{P}\left(\mathbf{T},\ \boldsymbol{\mathcal{V}}_{\Sigma_{k-1}}(U)\right)\right) \\ &= \operatorname{tr}(\mathbf{T}) - \operatorname{tr}(\mathbf{T}) = 0 \qquad\qquad (k = 2, \ldots, 6).\end{aligned} \tag{78}$$

Hence the eigenvalues of $\mathbf{Q}_{\Sigma_k}(\mathbf{T}, U)$ cannot all be positive. Thus none of

$$\mathbf{Q}_\Sigma(\mathbf{T}, U), \quad \Sigma = \text{XISO, TET, ORTH, MONO, TRIV,} \tag{79}$$

is physically permissible. The Σ-percentages $q_\Sigma(\mathbf{T}, U)$ (Eq. (73)) are presumably impermissible as well.

13 The Symmetry Cartesian Coordinate System

On a first reading of Browaeys & Chevrot [9], their exposition seems to lack any counterpart to our $U \in \mathbb{U}$. Unlike our $\mathbf{Q}_\Sigma(\mathbf{T}, U)$, $\mathbf{P}(\mathbf{T}, \boldsymbol{\mathcal{V}}_\Sigma(U))$, $\mathbf{X}(\mathbf{T}, U)$, $p_\Sigma(\mathbf{T}, U)$, and $q_\Sigma(\mathbf{T}, U)$, their summands, projections, hexagonal approximations, and percentages do not appear to depend on U. The equivalent of U is there, however, implicit in their "symmetry cartesian coordinate system" (SCCS) for 3-space.

The SCCS for an elastic map $\mathbf{T}$ is determined by a rotation matrix $U \in \mathbb{U}$. The basis vectors in the SCCS are $U\mathbf{e}_1$, $U\mathbf{e}_2$, $U\mathbf{e}_3$; they are the columns of U. If the symmetry class $\Sigma_\mathbf{T} \neq$ TRIV, MONO, the matrix U is supposed to be chosen so that the matrix for $\mathbf{T}$ in the SCCS coordinates becomes, in our terminology, a $\Sigma_\mathbf{T}$ reference matrix.[5] From our Eq. (52b), Browaeys & Chevrot are thus requiring U to be a $\Sigma_\mathbf{T}$-minimizer for $\mathbf{T}$. Hence the regular axes of their XISO-approximations are high symmetry axes of $\mathbf{T}$, as is the case for $\mathbf{B}$ in our Fig. 10, for example.

If $\Sigma_\mathbf{T}$ is TRIV or MONO, Browaeys & Chevrot [9, p 670] specify U by what we will refer to as the Bisectrix Rule:

> ... the three SCCS directions are chosen as the bisectrix of each pair of one d_{ij} eigenvector and the corresponding closest v_{ik} eigenvector.

In (our) Fig. 9, where $\Sigma_\mathbf{T} =$ ORTH, the requirement that U be a $\Sigma_\mathbf{T}$-minimizer for $\mathbf{T}$ gave the XISO-approximations $\mathbf{B}_1$, $\mathbf{B}_2$, $\mathbf{B}_3$, but it cannot give the closest XISO maps $\mathbf{K}_1$ and $\mathbf{K}_2$ to $\mathbf{T}$. The figure is consistent with the ORTH diagram in Fig. 5.

In Fig. 10, where $\Sigma_\mathbf{T} =$ TET, the requirement that U be a $\Sigma_\mathbf{T}$-minimizer for $\mathbf{T}$ gave the XISO-approximation $\mathbf{B}$, but it cannot give the closest XISO maps $\mathbf{K}_1$ and $\mathbf{K}_2$ to $\mathbf{T}$. The figure is consistent with the TET diagram in Fig. 5.

In Fig. 11, where again $\Sigma_\mathbf{T} =$ TET, the requirement that U be a $\Sigma_\mathbf{T}$-minimizer for $\mathbf{T}$ gave the XISO-approximation $\mathbf{B}$, but it cannot give the closest XISO maps $\mathbf{K}_1$, $\mathbf{K}_2$, $\mathbf{K}_3$, $\mathbf{K}_4$. The map $\mathbf{B}$ turned out to be isotropic. The figure is consistent with the TET diagram in Fig. 5.

In Figs. 7, 8, and 12, where $\Sigma_\mathbf{T}$ is MONO or TRIV, we relied on the code `MS_axes.m` [57] to implement the Bisectrix Rule. (Our matrices $[\mathbf{T}]_{\mathbb{B}\mathbb{B}}$ must be converted to Voigt matrices for use in `MS_axes`. In the notation of `MS_axes` our U is $(RR)^\top$, but in $\mathbf{X}(\mathbf{T}, U)$ the

[5] For Browaeys & Chevrot [9], matrix representations of elastic maps are Voigt matrices rather than representations with respect to our basis $\mathbb{B}$, and their reference matrices would differ from those in our Eq. (81). To go back and forth between the two representations, use [53, Eqs. S28 and S29].

matrix U can always be replaced by UG, where $G \in \mathbb{U}_{\text{XISO}}$.) In none of those figures did the Bisectrix Rule find a rotation matrix U that led to a closest XISO map to $\mathbf{T}$.

Figures 7–12 are not typical, but they show that the SCCS cannot be relied on to find a closest XISO map to a given $\mathbf{T}$.

In Sect. 12.2, where we calculated Σ-percentages for an orthorhombic $\mathbf{T}$, we chose U so as to be consistent with the SCCS, though we see no conceptual justification for doing so. In our terms, the rotations $U = I, U_{\mathbf{i}}, U_{\mathbf{j}}$ were $\Sigma_{\mathbf{T}}$-minimizers for $\mathbf{T}$. For those three rotations, Eq. (77e) gave three distinct 6-tuples of Σ-percentages—an impossibility if the notion of Σ-percentage were to have any meaning.

14 Literature Citing Browaeys and Chevrot (2004)

As of January 2024, the paper of Browaeys and Chevrot (BC) [9] had been cited by 136 journal articles. Here we focus on the subset of 62 studies where BC was more significant, with the two main applications being to XISO-approximations and to Σ-percentages.

The three main software packages cited are D-Rex [33] (20 studies), MSAT [60] (12 studies), and MTEX [2] (8 studies), but there are also several modified or alternative versions [25, 29, 32, 34, 35, 41, 42, 51].

The BC XISO-approximation is used in 27 of the 62 studies. These studies calculate elastic properties of mantle and crustal Earth materials based on a combination of factors, including mineralogical compositions, rheological models, geodynamical flow models, and global models of plate configuration and plate motion. The calculated elastic properties have symmetries ranging from trivial to orthorhombic, and the authors use the BC XISO-approximation for purposes of interpretation and visualization. Among these 27 studies there are 13 that cite D-Rex [3, 4, 14, 21–23, 31, 33, 40, 45, 46, 55, 56], four that cite a modified version of D-Rex [32, 34, 35, 41], two that cite MTEX [27, 28], and eight that cite none of the three codes [5, 17, 30, 44, 47, 48, 52, 62]. D-Rex [33], coauthored by Browaeys, is meant to perform the XISO-approximation of [9].

The BC decomposition is performed in 27 of the 62 studies [1, 3, 6, 7, 10–13, 16, 26, 29–31, 36–39, 42, 43, 48–50, 52, 60, 61, 63, 64]. Among these 27 studies there are 18 that calculate Σ-percentages. There are eight that use MSAT for the decomposition [16, 39, 63] or for Σ-percentages [11–13, 26, 60]. There are 18 studies that have a figure or table based on the BC decomposition.

A few authors express reservations about the BC theory. Lisboa et al. [38] mention that the summands in the BC decomposition are not positive definite: "…the decomposed symmetries are fictitious materials that hold only the properties of a specific symmetry. They do not represent any natural or synthetic materials." Brownlee et al. [10] point out that the trigonal symmetry class is not included in the BC decomposition. Regarding the Σ-percentages, Bernard et al. [7] write that "…when we look at the decomposition results for a single crystal of olivine, we see that even here the approach of [9] gives us a large hexagonal component, even though olivine itself is an orthorhombic mineral."

We mention the many computer codes above only to suggest that there may have been undue reliance on codes. Our assessment of Browaeys and Chevrot [9] does not depend on results from these codes.

15 Conclusion

Except when $\Sigma = \text{ISO}$ or $\Sigma = \text{TRIV}$, the set $\mathcal{T}_\Sigma$ of elastic maps with symmetry class at least Σ (orange surface in Fig. 1) is not a subspace of $\mathcal{T}$, since the sum of two elastic maps in $\mathcal{T}_\Sigma$ need not be in $\mathcal{T}_\Sigma$. Orthogonal projection onto $\mathcal{T}_\Sigma$ therefore makes no sense.

Authors who talk about projection onto $\mathcal{T}_\Sigma$ are thus apt to be confused. They are probably projecting onto one of the subspaces $\mathcal{V}_\Sigma(U)$ of $\mathcal{T}_\Sigma$. The rotation matrix U may well be invisible in the exposition, but the XISO-approximations of an elastic map $\mathbf{T}$ and the Σ-percentages p_Σ and q_Σ depend on the projection and hence can be expected to depend on U (and $\mathbf{T}$). The allowable matrices U need to be drastically restricted if the notions of XISO-approximation and Σ-percentages are to be meaningful. The restriction should be consistent with the intended meaning of the notions; it cannot be just ad hoc.

Given an elastic map $\mathbf{T}$, we considered two competing rules for restricting U:

Rule 1: Require U to be an XISO-minimizer for $\mathbf{T}$. This makes the XISO-approximation $\mathbf{X}(\mathbf{T}, U)$ a closest XISO map to $\mathbf{T}$.

Rule 2: Require U to be a $\Sigma_\mathbf{T}$-minimizer for $\mathbf{T}$. This makes a regular axis of $\mathbf{X}(\mathbf{T}, U)$ coincide with a high symmetry axis of $\mathbf{T}$. If the symmetry class $\Sigma_\mathbf{T}$ of $\mathbf{T}$ is TET, for example, a regular axis of $\mathbf{X}(\mathbf{T}, U)$ would also be the 4-fold axis of $\mathbf{T}$, as for $\mathbf{B}$ in Fig. 10.

One might think that the two rules would be equivalent, and indeed for many $\mathbf{T}$ they are, but not for all $\mathbf{T}$, as shown in Figs. 7–11.

When it comes to XISO-approximations, we think "best" ought to be synonymous with "closest." Rule 1 is then the obvious choice. When $\Sigma_\mathbf{T} \neq \text{TRIV}, \text{MONO}$, Browaeys & Chevrot [9] use the equivalent of Rule 2. Our Figs. 9–11 show that in that case Browaeys & Chevrot [9] cannot be depended on to find a closest XISO map to a given $\mathbf{T}$.

When $\Sigma_\mathbf{T}$ is TRIV or MONO, Browaeys & Chevrot [9] specify U according to their Bisectrix Rule (our Sect. 13). (Rule 2 does nothing when $\Sigma_\mathbf{T} = \text{TRIV}$, since every $U \in \mathbb{U}$ is then a $\Sigma_\mathbf{T}$-minimizer for $\mathbf{T}$, by Eq. (51a).) Our Figs. 8 and 12 show that the Bisectrix Rule, like Rule 2, cannot be depended on to find a closest XISO map to a given $\mathbf{T}$.

Of all the symmetry classes, the trivial class is by far the most important in practice. If $\mathbf{T}$ arises through measurement, with no assumptions made about its symmetry, its symmetry will almost certainly be only trivial, due to uncertainties in the measurements. This makes the Bisectrix Rule much more than just an afterthought.

Like the XISO-approximations, the Σ-percentages p_Σ and q_Σ depend on U. If the percentages were to be meaningful, then U would have to be restricted somehow. But whereas there were some conceptually plausible guidelines for doing so in the case of XISO-approximations, we see nothing comparable for the Σ-percentages.

Regardless of how U is chosen, we think both p_Σ and q_Σ should be abandoned. We find nothing in the definition of $p_\Sigma(\mathbf{T}, U)$ (Eqs. (74a) and (74b)) that would justify referring to $p_\Sigma(\mathbf{T}, U)$ as the percentage of the symmetry Σ in $\mathbf{T}$. And although the definition $q_\Sigma(\mathbf{T}, U) = \|\mathbf{Q}_\Sigma(\mathbf{T}, U)\|^2/\|\mathbf{T}\|^2$ (Eq. (73)) clearly expresses $q_\Sigma(\mathbf{T}, U)$ as the (square of the) fraction of the Σ-summand in $\mathbf{T}$, the summand has no physical meaning for $\Sigma \neq \text{ISO}$ (Sect. 12.3).

In spite of the attention that we initially paid to the decomposition, and in spite of our title, the decomposition is nearly irrelevant. We used it only to show that its summands, with the possible exception of the ISO summand, are physically impermissible, and we used it in the definition of the (discredited) percentage $q_\Sigma(\mathbf{T}, U)$.

In conclusion, we recommend abandoning the Σ-percentages p_Σ and q_Σ, and we recommend abandoning the notion of XISO-approximation except when it coincides with the notion of closest XISO map. Note that finding the closest XISO map to $\mathbf{T}$ (Sect. 8) does not

require knowing the symmetry of $\mathbf{T}$, and it does not require the apparatus of Browaeys & Chevrot [9].

Appendix A: The Reference Matrices for the Basis $\mathbb{B}$

The basis $\mathbb{B}$ for $\mathbb{M}$ consists of the six matrices

$$B_1 = \frac{1}{\sqrt{2}}\begin{pmatrix} 0 & 0 & 0 \\ 0 & 0 & 1 \\ 0 & 1 & 0 \end{pmatrix}, \quad B_2 = \frac{1}{\sqrt{2}}\begin{pmatrix} 0 & 0 & 1 \\ 0 & 0 & 0 \\ 1 & 0 & 0 \end{pmatrix}, \quad B_3 = \frac{1}{\sqrt{2}}\begin{pmatrix} 0 & 1 & 0 \\ 1 & 0 & 0 \\ 0 & 0 & 0 \end{pmatrix},$$
$$B_4 = \frac{1}{\sqrt{2}}\begin{pmatrix} -1 & 0 & 0 \\ 0 & 1 & 0 \\ 0 & 0 & 0 \end{pmatrix}, \quad B_5 = \frac{1}{\sqrt{6}}\begin{pmatrix} 1 & 0 & 0 \\ 0 & 1 & 0 \\ 0 & 0 & -2 \end{pmatrix}, \quad B_6 = \frac{1}{\sqrt{3}}\begin{pmatrix} 1 & 0 & 0 \\ 0 & 1 & 0 \\ 0 & 0 & 1 \end{pmatrix}. \tag{80}$$

Using $\mathbb{B}$ simplifies the reference matrices and the projections. For the projections, compare Eqs. (84a)–(84h) with Appendix A of Browaeys & Chevrot [9] or with Sect. 4.2 of Diner et al. [19].

The reference matrices $T^{\mathbb{B}}_{\Sigma}$ for $\mathbb{B}$ are

$$T^{\mathbb{B}}_{\text{ISO}} = \begin{pmatrix} a & & & & & \\ & a & & & & \\ & & a & & & \\ & & & a & & \\ & & & & a & \\ & & & & & f \end{pmatrix}, \quad T^{\mathbb{B}}_{\text{XISO}} = \begin{pmatrix} a & & & & & \\ & a & & & & \\ & & c & & & \\ & & & c & & \\ & & & & e & k \\ & & & & k & f \end{pmatrix}, \quad T^{\mathbb{B}}_{\text{TET}} = \begin{pmatrix} a & & & & & \\ & a & & & & \\ & & c & & & \\ & & & d & & \\ & & & & e & k \\ & & & & k & f \end{pmatrix},$$

$$T^{\mathbb{B}}_{\text{ORTH}} = \begin{pmatrix} a & & & & & \\ & b & & & & \\ & & c & & & \\ & & & d & j & p \\ & & & j & e & k \\ & & & p & k & f \end{pmatrix}, \quad T^{\mathbb{B}}_{\text{MONO}} = \begin{pmatrix} a & g & & & & \\ g & b & & & & \\ & & c & i & o & s \\ & & i & d & j & p \\ & & o & j & e & k \\ & & s & p & k & f \end{pmatrix}, \quad T^{\mathbb{B}}_{\text{TRIV}} = \begin{pmatrix} a & g & m & q & t & v \\ g & b & h & n & r & u \\ m & h & c & i & o & s \\ q & n & i & d & j & p \\ t & r & o & j & e & k \\ v & u & s & p & k & f \end{pmatrix},$$

$$T^{\mathbb{B}}_{\text{CUBE}} = \begin{pmatrix} a & & & & & \\ & a & & & & \\ & & a & & & \\ & & & d & & \\ & & & & d & \\ & & & & & f \end{pmatrix}, \quad T^{\mathbb{B}}_{\text{TRIG}} = \begin{pmatrix} a & 0 & m & 0 & & \\ 0 & a & 0 & m & & \\ m & 0 & c & 0 & & \\ 0 & m & 0 & c & & \\ & & & & e & k \\ & & & & k & f \end{pmatrix}. \tag{81}$$

The fundamental relation between the reference matrix $T^{\mathbb{B}}_{\Sigma}$ and the reference group $\mathbb{U}_{\Sigma}$ is that the symmetry group $\mathcal{S}_{\mathbf{T}}$ of an elastic map $\mathbf{T}$ is at least $\mathbb{U}_{\Sigma}$ if and only if the matrix representation of $\mathbf{T}$ with respect to $\mathbb{B}$ has the form of the reference matrix $T^{\mathbb{B}}_{\Sigma}$:

$$\mathcal{S}_{\mathbf{T}} \supset \mathbb{U}_{\Sigma} \iff [\mathbf{T}]_{\mathbb{B}\mathbb{B}} = T^{\mathbb{B}}_{\Sigma}(a, b, \ldots) \text{ for some } a, b, \ldots \tag{82}$$

With computer help on the algebra, Eq. (82) is verified rather easily. For $\Sigma = \text{TET}$, for example, the solution to the equation $[\overline{Z_{\pi/2}}]\, T^{\mathbb{B}}_{\text{ORTH}}\, [\overline{Z_{\pi/2}}]^{\top} = T^{\mathbb{B}}_{\text{ORTH}}$ is found to be $b = a$, $j = p = 0$, which then gives $T^{\mathbb{B}}_{\text{TET}}$ from $T^{\mathbb{B}}_{\text{ORTH}}$. The only case that requires care is $\Sigma = \text{TRIG}$. One first finds the matrix $T^{\mathbb{B}}_{\text{MONOY}}$ for elastic maps having 2-fold axes in the y-direction. Then one solves the equation $[\overline{Z_{2\pi/3}}]\, T^{\mathbb{B}}_{\text{MONOY}}\, [\overline{Z_{2\pi/3}}]^{\top} = T^{\mathbb{B}}_{\text{MONOY}}$. The solution gives $T^{\mathbb{B}}_{\text{TRIG}}$ from $T^{\mathbb{B}}_{\text{MONOY}}$.

From Eqs. (15), (29), (82), the form of the reference matrix $T^{\mathbb{B}}_{\Sigma}$ characterizes membership in the subspace $\boldsymbol{\mathcal{V}}_{\Sigma}(I)$:

$$\mathcal{V}^{\mathbb{B}}_{\Sigma}(I) = \left\{ T : T = T^{\mathbb{B}}_{\Sigma}(a, b, \ldots) \text{ for some } a, b, \ldots \right\}. \tag{83a}$$

Then from Eq. (20),

$$\mathcal{V}^{\mathbb{B}}_{\Sigma}(U) = \left\{ T : T = [\overline{U}]_{\mathbb{B}\mathbb{B}}\, T^{\mathbb{B}}_{\Sigma}(a, b, \ldots)\, [\overline{U}]^{\top}_{\mathbb{B}\mathbb{B}} \text{ for some } a, b, \ldots \right\}. \tag{83b}$$

Appendix B: The Projections to $\mathcal{V}^{\mathbb{B}}_{\Sigma}(I)$

The subspace $\mathcal{V}^{\mathbb{B}}_{\Sigma}(I)$ consists of the 6×6 matrices that have the form of the reference matrix $T^{\mathbb{B}}_{\Sigma}$. One verifies Eqs. (84a)–(84h) using Eqs. (1a) and (1b).

For $T = T^{\mathbb{B}}_{\text{TRIV}}$ the projection of T to $\mathcal{V}^{\mathbb{B}}_{\Sigma}(I)$ is

$$P(T, \mathcal{V}^{\mathbb{B}}_{\text{ISO}}(I)) = \begin{pmatrix} a' & & & & & \\ & a' & & & & \\ & & a' & & & \\ & & & a' & & \\ & & & & a' & \\ & & & & & f \end{pmatrix}, \qquad a' = \frac{a+b+c+d+e}{5}, \tag{84a}$$

$$P(T, \mathcal{V}^{\mathbb{B}}_{\text{XISO}}(I)) = \begin{pmatrix} a' & & & & & \\ & a' & & & & \\ & & c' & & & \\ & & & c' & & \\ & & & & e & k \\ & & & & k & f \end{pmatrix}, \qquad \begin{aligned} a' &= \frac{a+b}{2}, \\ c' &= \frac{c+d}{2}, \end{aligned} \tag{84b}$$

$$P(T, \mathcal{V}^{\mathbb{B}}_{\text{TET}}(I)) = \begin{pmatrix} a' & & & & & \\ & a' & & & & \\ & & c & & & \\ & & & d & & \\ & & & & e & k \\ & & & & k & f \end{pmatrix}, \qquad a' = \frac{a+b}{2}, \tag{84c}$$

$$P(T, \mathcal{V}^{\mathbb{B}}_{\text{ORTH}}(I)) = \begin{pmatrix} a & & & & & \\ & b & & & & \\ & & c & & & \\ & & & d & j & p \\ & & & j & e & k \\ & & & p & k & f \end{pmatrix}, \tag{84d}$$

$$P(T,\mathcal{V}^{\mathbb{B}}_{\text{MONO}}(I)) = \begin{pmatrix} a & g & & & & \\ g & b & & & & \\ & & c & i & o & s \\ & & i & d & j & p \\ & & o & j & e & k \\ & & s & p & k & f \end{pmatrix}, \tag{84e}$$

$$P(T,\mathcal{V}^{\mathbb{B}}_{\text{TRIV}}(I)) = T, \tag{84f}$$

$$P(T,\mathcal{V}^{\mathbb{B}}_{\text{CUBE}}(I)) = \begin{pmatrix} a' & & & & & \\ & a' & & & & \\ & & a' & & & \\ & & & d' & & \\ & & & & d' & \\ & & & & & f \end{pmatrix}, \qquad \begin{aligned} a' &= \frac{a+b+c}{3}, \\ d' &= \frac{d+e}{2}, \end{aligned} \tag{84g}$$

$$P(T,\mathcal{V}^{\mathbb{B}}_{\text{TRIG}}(I)) = \begin{pmatrix} a' & 0 & m' & 0 & & \\ 0 & a' & 0 & m' & & \\ m' & 0 & c' & 0 & & \\ 0 & m' & 0 & c' & & \\ & & & & e & k \\ & & & & k & f \end{pmatrix}, \qquad \begin{aligned} a' &= \frac{a+b}{2}, \\ c' &= \frac{c+d}{2}, \\ m' &= \frac{m+n}{2}. \end{aligned} \tag{84h}$$

Appendix A of Browaeys & Chevrot [9] is consistent with our Eqs. (84a)–(84e). In our terms, Browaeys & Chevrot are projecting onto $\mathcal{V}^{\mathbb{B}}_{\Sigma}(I)$.

For any elastic map $\mathbf{S}$, we let $\text{tr}_5(\mathbf{S})$ (the "five-trace" of $\mathbf{S}$) be the sum of the first five diagonal entries of $[\mathbf{S}]_{\mathbb{BB}}$, and we let $f(\mathbf{S})$ be the sixth diagonal entry. Then from Eqs. (19) and (84a),

$$\big[\mathbf{P}_{\text{ISO}}\big(\mathbf{P}\big(\mathbf{T},\boldsymbol{\mathcal{V}}_{\Sigma}(U)\big)\big)\big]_{\mathbb{BB}} = [\mathbf{P}_{\text{ISO}}(\mathbf{T})]_{\mathbb{BB}},$$

$$\begin{pmatrix} \frac{1}{5}\text{tr}_5(\mathbf{P}) & & & & & \\ & \frac{1}{5}\text{tr}_5(\mathbf{P}) & & & & \\ & & \frac{1}{5}\text{tr}_5(\mathbf{P}) & & & \\ & & & \frac{1}{5}\text{tr}_5(\mathbf{P}) & & \\ & & & & \frac{1}{5}\text{tr}_5(\mathbf{P}) & \\ & & & & & f(\mathbf{P}) \end{pmatrix} = \begin{pmatrix} \frac{1}{5}\text{tr}_5(\mathbf{T}) & & & & & \\ & \frac{1}{5}\text{tr}_5(\mathbf{T}) & & & & \\ & & \frac{1}{5}\text{tr}_5(\mathbf{T}) & & & \\ & & & \frac{1}{5}\text{tr}_5(\mathbf{T}) & & \\ & & & & \frac{1}{5}\text{tr}_5(\mathbf{T}) & \\ & & & & & f(\mathbf{T}) \end{pmatrix}, \tag{85}$$

where $\mathbf{P} = \mathbf{P}\big(\mathbf{T},\boldsymbol{\mathcal{V}}_{\Sigma}(U)\big)$. Thus both tr_5 and f are invariant under projection to $\boldsymbol{\mathcal{V}}_{\Sigma}(U)$:

$$\text{tr}_5\Big(\mathbf{P}\big(\mathbf{T},\boldsymbol{\mathcal{V}}_{\Sigma}(U)\big)\Big) = \text{tr}_5(\mathbf{T}) \qquad (U \in \mathbb{U},\ \text{all } \Sigma), \tag{86a}$$

$$f\Big(\mathbf{P}\big(\mathbf{T},\boldsymbol{\mathcal{V}}_{\Sigma}(U)\big)\Big) = f(\mathbf{T}) \qquad (U \in \mathbb{U},\ \text{all } \Sigma). \tag{86b}$$

The trace is then invariant as well:

$$\text{tr}\Big(\mathbf{P}\big(\mathbf{T},\boldsymbol{\mathcal{V}}_{\Sigma}(U)\big)\Big) = \text{tr}(\mathbf{T}). \tag{87}$$

Appendix C: Proofs of Eqs. (24a), (30), (42)

C.1 Proof of Eq. (24a)

$$\mathbf{P}\big(\mathbf{T},\, \overline{U} \circ \boldsymbol{\mathcal{V}} \circ \overline{U}^*\big) = \overline{U} \circ \mathbf{P}\big(\mathbf{A}, \boldsymbol{\mathcal{V}}\big) \circ \overline{U}^*. \tag{24a}$$

Proof Let

$$\mathbf{T}_1 = \mathbf{P}\big(\mathbf{A}, \boldsymbol{\mathcal{V}}\big). \tag{88}$$

We want to show

$$\overline{U} \circ \mathbf{T}_1 \circ \overline{U}^* \in \overline{U} \circ \boldsymbol{\mathcal{V}} \circ \overline{U}^*, \tag{89a}$$

$$\mathbf{T} - \overline{U} \circ \mathbf{T}_1 \circ \overline{U}^* \in \Big(\overline{U} \circ \boldsymbol{\mathcal{V}} \circ \overline{U}^*\Big)^{\perp}. \tag{89b}$$

From Eqs. (88), (1a), (20),

$$\mathbf{T}_1 \in \boldsymbol{\mathcal{V}},$$
$$\overline{U} \circ \mathbf{T}_1 \circ \overline{U}^* \in \overline{U} \circ \boldsymbol{\mathcal{V}} \circ \overline{U}^*.$$

This proves Eq. (89a).

From Eqs. (88), (1b), (24b), (20),

$$\mathbf{A} - \mathbf{T}_1 \in \boldsymbol{\mathcal{V}}^{\perp},$$
$$\overline{U} \circ \mathbf{A} \circ \overline{U}^* - \overline{U} \circ \mathbf{T}_1 \circ \overline{U}^* \in \overline{U} \circ \boldsymbol{\mathcal{V}}^{\perp} \circ \overline{U}^*,$$
$$\mathbf{T} - \overline{U} \circ \mathbf{T}_1 \circ \overline{U}^* \in \Big(\overline{U} \circ \boldsymbol{\mathcal{V}} \circ \overline{U}^*\Big)^{\perp}.$$

This proves Eq. (89b).

C.2 Proof of Eq. (30)

$$\big[\mathbf{P}\big(\mathbf{T}, \boldsymbol{\mathcal{V}}_{\Sigma}(U)\big)\big] = P\big(T, \mathcal{V}_{\Sigma}^{\mathbb{B}}(U)\big). \tag{30}$$

Proof We abbreviate $\boldsymbol{\mathcal{V}}_{\Sigma}(U)$ and $\mathcal{V}_{\Sigma}^{\mathbb{B}}(U)$ to $\boldsymbol{\mathcal{V}}$ and $\mathcal{V}$, respectively. We let $\mathbf{T}_1 = \mathbf{P}(\mathbf{T}, \boldsymbol{\mathcal{V}})$ and $T_1 = [\mathbf{T}_1]_{\mathbb{BB}}$. Then, with the first line coming from Eqs. (1a) and (1b),

$$\begin{aligned}
&\mathbf{T}_1 \in \boldsymbol{\mathcal{V}} \quad \text{and} \quad \mathbf{T} - \mathbf{T}_1 \in \boldsymbol{\mathcal{V}}^{\perp},\\
&T_1 \in \mathcal{V} \quad \text{and} \quad [\mathbf{T} - \mathbf{T}_1] \in \mathcal{V}^{\perp},\\
&T_1 \in \mathcal{V} \quad \text{and} \quad T - T_1 \in \mathcal{V}^{\perp},\\
&T_1 = P(T, \mathcal{V}),\\
&[\mathbf{P}(\mathbf{T}, \boldsymbol{\mathcal{V}})] = P(T, \mathcal{V}).
\end{aligned}$$

C.3 Proof of Eq. (42)

$$\left.\begin{aligned} \mathbf{T} &= \sum_{k=1}^{6} \mathbf{Q}_k \\ \mathbf{Q}_k &\in \boldsymbol{\mathcal{V}}_{\Sigma_k}(U) \cap \left(\boldsymbol{\mathcal{V}}_{\Sigma_{k-1}}(U)\right)^{\perp} \end{aligned}\right\} \Longrightarrow \mathbf{Q}_k = \mathbf{Q}_{\Sigma_k}(\mathbf{T}, U). \tag{42}$$

Proof Assume the hypotheses in Eq. (42). Again abbreviating $\boldsymbol{\mathcal{V}}_{\Sigma_k}(U)$ to $\boldsymbol{\mathcal{V}}_k$, we first show

$$\mathbf{P}(\mathbf{Q}_i, \boldsymbol{\mathcal{V}}_k) = \begin{cases} \mathbf{Q}_i & i \le k, \quad (90a) \\ \mathbf{0} & i > k. \quad (90b) \end{cases}$$

If $i \le k$ then $\mathbf{Q}_i \in \boldsymbol{\mathcal{V}}_i \subset \boldsymbol{\mathcal{V}}_k$, so $\mathbf{P}(\mathbf{Q}_i, \boldsymbol{\mathcal{V}}_k) = \mathbf{Q}_i$, which is Eq. (90a). If $i > k$ then

$$\begin{aligned} \mathbf{Q}_i - \mathbf{P}(\mathbf{Q}_i, \boldsymbol{\mathcal{V}}_k) &\in \boldsymbol{\mathcal{V}}_k^{\perp} && \text{(from Eq. (1b))}, \\ \mathbf{Q}_i &\in \boldsymbol{\mathcal{V}}_k^{\perp} && \text{(from given and Eq. (34a))}, \\ \mathbf{P}(\mathbf{Q}_i, \boldsymbol{\mathcal{V}}_k) &\in \boldsymbol{\mathcal{V}}_k^{\perp}, \\ \mathbf{P}(\mathbf{Q}_i, \boldsymbol{\mathcal{V}}_k) &\in \boldsymbol{\mathcal{V}}_k && \text{(from Eq. (1a))}, \\ \mathbf{P}(\mathbf{Q}_i, \boldsymbol{\mathcal{V}}_k) &= \mathbf{0}, \end{aligned} \tag{91}$$

which is Eq. (90b).

Then

$$\begin{aligned} \mathbf{T} &= \mathbf{Q}_1 + \cdots + \mathbf{Q}_6, \\ \mathbf{P}(\mathbf{T}, \boldsymbol{\mathcal{V}}_k) &= \mathbf{P}(\mathbf{Q}_1, \boldsymbol{\mathcal{V}}_k) + \cdots + \mathbf{P}(\mathbf{Q}_6, \boldsymbol{\mathcal{V}}_k), \\ &= \mathbf{Q}_1 + \cdots + \mathbf{Q}_{k-1} + \mathbf{Q}_k, \\ \mathbf{P}(\mathbf{T}, \boldsymbol{\mathcal{V}}_{k-1}) &= \mathbf{Q}_1 + \cdots + \mathbf{Q}_{k-1}, \\ \mathbf{Q}_k &= \mathbf{P}(\mathbf{T}, \boldsymbol{\mathcal{V}}_k) - \mathbf{P}(\mathbf{T}, \boldsymbol{\mathcal{V}}_{k-1}) = \mathbf{Q}_{\Sigma_k}(\mathbf{T}, U). \end{aligned} \tag{92}$$

Appendix D: Matrices for Sects. 7 and 8

The matrix for $\mathbf{T}$ in Figs. 3 and 4 is

$$T = [\mathbf{T}]_{\mathbb{BB}} = \begin{pmatrix} 206.2 & -67.4 & 17.1 & -15.9 & 166.6 & -19.5 \\ -67.4 & 352.9 & 32.2 & 3.3 & 61.6 & -41.6 \\ 17.1 & 32.2 & 343.8 & 0.4 & 73.6 & -4.2 \\ -15.9 & 3.3 & 0.4 & 270.0 & 88.8 & 13.3 \\ 166.6 & 61.6 & 73.6 & 88.8 & 287.1 & 30.7 \\ -19.5 & -41.6 & -4.2 & 13.3 & 30.7 & 74.0 \end{pmatrix}. \tag{93}$$

To get the rotation matrix U in Fig. 3 we first found the Voigt matrix of $\mathbf{T}$ using [53, Eq. S29]. From it, we used `MS_axes` [57] to get[6]

$$U = \begin{pmatrix} 0.807 & -0.295 & 0.512 \\ 0.228 & 0.955 & 0.192 \\ -0.545 & -0.038 & 0.838 \end{pmatrix} \qquad \text{(in Fig. 3).} \tag{94}$$

(We actually ran `MS_axes` twice—once with the option `X3_stiff` and once without—and thus got two rotation matrices. We used the one that gave the better of the two XISO-approximations.)

The matrix U in Fig. 4, from Eqs. (46), (33), (84b), is

$$U = \begin{pmatrix} 0.893 & 0.423 & 0.153 \\ -0.441 & 0.758 & 0.481 \\ 0.088 & -0.497 & 0.864 \end{pmatrix} \qquad \text{(in Fig. 4).} \tag{95}$$

From Eqs. (31a), (31b), (93), (95), the matrix for $\mathbf{T}'$ in Fig. 4 is

$$T' = [\mathbf{T}']_{\mathbb{BB}} = \begin{pmatrix} 194.9 & -62.0 & -22.3 & -0.9 & 162.5 & -29.2 \\ -62.0 & 370.6 & 43.1 & -35.7 & 51.6 & -9.3 \\ -22.3 & 43.1 & 317.1 & -10.0 & 45.8 & -5.2 \\ -0.9 & -35.7 & -10.0 & 310.0 & 64.9 & -7.3 \\ 162.5 & 51.6 & 45.8 & 64.9 & 267.5 & 25.1 \\ -29.2 & -9.3 & -5.2 & -7.3 & 25.1 & 74.0 \end{pmatrix} \qquad \text{(in Fig. 4).} \tag{96}$$

Acknowledgements We thank Aakash Gupta, who has implemented the minimization (Eq. (45)) in Python and has run it on many elastic maps as a check on our Mathematica routine. We thank Brandon VanderBeek and Thorsten Becker for discussions regarding the software MSAT and DREX. We thank editor Chi-Sing Man for overseeing our paper, and we thank two anonymous reviewers.

Author contributions W.T. wrote the manuscript and prepared the figures. C.T. performed the literature review, reviewed the manuscript, and performed calculations in MSAT (Matlab), DREX (Fortran), and Mathematica software.

Funding C. Tape was supported by National Science Foundation grant EAR 2342129.

Code Availability Mathematica code for finding Σ-minimizers (`ES_FindSymGroups.nb`) and for drawing contour plots of $\alpha^{\mathbf{T}}_{\text{MONO}}$ (`ES_ContourPlots.nb`) is available at https://github.com/carltape/mtbeach

Declarations

Competing interests The authors declare no competing interests.

[6] $U = U_{\text{MSAT}} Y_\pi Z_{-2\pi/9}$, where U_{MSAT} is from `MS_axes`. The matrices U and U_{MSAT} produce the same XISO-approximation, due to Theorem 2. We chose U rather than U_{MSAT} so as to make the rotation in Fig. 3 more transparent.

References

1. Angus, D.A., Fisher, Q.J., Segura, J.M., Verdon, J.P., Kendall, J.M., Dutko, M., Crook, A.J.L.: Reservoir stress path and induced seismic anisotropy: results from linking coupled fluid-flow/geomechanical simulation with seismic modelling. Petroleum Science **13**, 669–684 (2016). https://doi.org/10.1007/s12182-016-0126-1
2. Bachmann, F., Rielscher, R., Schaeben, H.: Texture analysis with MTEX – free and open source software toolbox. Solid State Phenom. **160**, 63–68 (2010). https://doi.org/10.4028/www.scientific.net/SSP.160.63
3. Becker, T.W., Chevrot, S., Schulte-Pelkum, V., Blackman, D.K.: Statistical properties of seismic anisotropy predicted by upper mantle geodynamic models. J. Geophys. Res. **111**, B08309 (2006). https://doi.org/10.1029/2005JB004095
4. Becker, T.W., Schulte-Pelkum, V., Blackman, D.K., Kellogg, J.B., O'Connell, R.J.: Mantle flow under the western United States from shear wave splitting. Earth Planet. Sci. Lett. **247**, 235–251 (2006). https://doi.org/10.1016/j.epsl.2006.05.010
5. Becker, T.W., Lebedev, S., Long, M.D.: On the relationship between azimuthal anisotropy from shear wave splitting and surface wave tomography. J. Geophys. Res. **117 B**, 01306 (2012). https://doi.org/10.1029/2011JB008705
6. Beller, S., Chevrot, S.: Probing depth and lateral variations of upper-mantle seismic anisotropy from full-waveform inversion of teleseismic body-waves. Geophys. J. Int. **222**, 352–387 (2020). https://doi.org/10.1093/gji/ggaa069
7. Bernard, R.E., Schulte-Pelkum, V., Behr, W.M.: The competing effects of olivine and orthopyroxene CPO on seismic anisotropy. Tectonophysics **814**, 228954 (2021). https://doi.org/10.1016/j.tecto.2021.228954
8. Bóna, A., Bucataru, I., Slawinski, M.A.: Coordinate-free characterization of the symmetry classes of elastic tensors. J. Elast. **87**, 109–132 (2007)
9. Browaeys, J.T., Chevrot, S.: Decomposition of the elastic tensor and geophysical applications. Geophys. J. Int. **159**, 667–678 (2004). https://doi.org/10.1111/j.1365-246X.2004.02415.x
10. Brownlee, S.J., Schulte-Peljum, V., Raju, A., Mahan, K., Condit, C., Orlandini, O.F.: Characteristics of deep crustal seismic anisotropy from a compilation of rock elasticity tensors and their expression in receiver functions. Tectonics **36**, 1835–1857 (2017). https://doi.org/10.1002/2017TC004625
11. Colabella, L., Cisilino, A.P., Häiat, G., Kowalczyk, P.: Mimetization of the elastic properties of cancellous bone via a parameterized cellular material. Biomech. Model. Mechanobiol. **16**, 1485–1502 (2017). https://doi.org/10.1007/s10237-017-0901-y
12. Colabella, L., Pino, A.A.I., Ballarre, J., Kowalczyk, P., Cisilino, A.P.: Calculation of cancellous bone elastic properties with the polarization-based FFT iterative scheme. Int. J. Numer. Methods Biomed. Eng. **33**, e2879 (2017). https://doi.org/10.1002/cnm.2879
13. Colabella, L., Cisilino, A.P., Fachinotti, V., Kowalczyk, P.: An efficient strategy to implement local porosity constraints in the multiscale design of solids with parameterized biomimetic microstructures. Comput. Struct. **285**, 1–13 (2023). https://doi.org/10.1016/j.compstruc.2023.107084
14. Confal, J.M., Bezada, M.J., Eken, T., Faccenda, M., Saygin, E., Taymaz, T.: Influence of upper mantle anisotropy on isotropic P-wave tomography images obtained in the eastern Mediterranean region. J. Geophys. Res., Solid Earth **125**, 1–21 (2020). https://doi.org/10.1029/2019JB018559
15. Cowin, S.C., Mehrabadi, M.M.: On the identification of material symmetry for anisotropic elastic materials. Q. J. Mech. Appl. Math. **40**, 451–476 (1987)
16. Creasy, N., Pisconti, A., Long, M.D., Thomas, C.: Modeling of seismic anisotropy observations reveals plausible lowermost mantle flow directions beneath Siberia. Geochem. Geophys. Geosyst. **22**, 1–23 (2021). https://doi.org/10.1029/2021GC009924
17. de Jong, M., Olmstead, D.L., van de Walle, A., Asta, M.: First-principles study of the structural and elastic properties of rhenium-based transition-metal alloys. Phys. Rev. B **86**, 1 (2012). https://doi.org/10.1103/PhysRevB.86.224101

18. Dellinger, J.: Computing the optimal transversely isotropic approximation of a general elastic tensor. Geophysics **70**(5), i1–i10 (2005). https://doi.org/10.1190/1.2073890
19. Diner, Ç., Kochetov, M., Slawinski, M.A.: On choosing effective symmetry classes for elasticity tensors. Q. J. Mech. Appl. Math. **64**(1), 57–74 (2010)
20. Diner, Ç., Kochetov, M., Slawinski, M.A.: Identifying symmetry classes of elasticity tensors using monoclinic distance function. J. Elast. **102**, 175–190 (2011)
21. Faccenda, M.: Mid mantle seismic anisotropy around subduction zones. Phys. Earth Planet. Inter. **227**, 1–19 (2014). https://doi.org/10.1016/j.pepi.2013.11.015
22. Faccenda, M., Capitanio, F.A.: Seismic anisotropy around subduction zones: insights from three-dimensional modeling of upper mantle deformation and SKS splitting calculations. Geochem. Geophys. Geosyst. **14**(1), 243–262 (2013). https://doi.org/10.1002/ggge.20055
23. Faccenda, M., VanderBeek, B.P.: On constraining 3D seismic anisotropy in subduction, mid-ocean-ridge, and plume environments with teleseismic body wave data. J. Geodyn. **158**, 1–16 (2023). https://doi.org/10.1016/j.jog.2023.102003
24. Forte, S., Vianello, M.: Symmetry classes for elasticity tensors. J. Elast. **43**, 81–108 (1996)
25. Fraters, M.R.T., Billen, M.I.: On the implementation and usability of crystal preferred orientation evolution in geodynamic modeling. Geochem. Geophys. Geosyst. **22**, 1–27 (2021). https://doi.org/10.1029/2021GC009846
26. Frayssinet, E.E., Colabella, L., Cisilino, A.P.: Design and assessment of the biomimetic capabilities of a Voronoi-based cancellous microstructure. J. Mech. Behav. Biomed. Mater. **130**, 105186 (2022). https://doi.org/10.1016/j.jmbbm.2022.105186
27. Frothingham, M.G., Mahan, K.H., Schulte-Pelkum, V., Caine, J.S., Vollmer, F.W.: From crystals to crustal-scale seismic anisotropy: bridging the gap between rocks and seismic studies with digital geologic map data in Colorado. Tectonics **41**, 1–24 (2022). https://doi.org/10.1029/2021TC006893
28. Frothingham, M.G., Mahan, K.H., Schulte-Pelkum, V., Goncalves, P., Zucali, M.: Confronting solid-state shear bias: magmatic fabric contribution to crustal seismic anisotropy. Geophys. Res. Lett. **50**, 1–10 (2023). https://doi.org/10.1029/2022GL102399
29. Furstoss, J., Sarrazola, D.A.R., Bernacki, M., Muñoz, D.P.: Handling tensors using tensorial Kelvin bases: application to olivine polycrystal deformation modeling using elastically anistropic CPFEM. Comput. Mech. **67**, 955–967 (2021). https://doi.org/10.1007/s00466-021-01976-9
30. He, Y.X., Angus, D.A., Yuan, S.Y., Xu, Y.G.: Feasibility of time-lapse AVO and AVOA analysis to monitor compaction-induced seismic anisotropy. J. Appl. Geophys. **122**, 134–148 (2015). https://doi.org/10.1016/j.jappgeo.2015.09.010
31. Hedjazian, N., Kaminski, E.: Defining a proxy for the interpretation of seismic anisotropy in non-Newtonian mantle flows. Geophys. Res. Lett. **41**, 7065–7072 (2014). https://doi.org/10.1002/2014GL061372
32. Hu, J., Faccenda, M., Liu, L.: Subduction-controlled mantle flow and seismic anisotropy in South America. Earth Planet. Sci. Lett. **470**, 13–24 (2017). https://doi.org/10.1016/j.epsl.2017.04.027
33. Kaminski, E., Ribe, N.M., Browaeys, J.T.: D-Rex, a program for calculation of seismic anisotropy due to crystal lattice preferred orientation in the convective upper mantle. Geophys. J. Int. **158**, 744–752 (2004). https://doi.org/10.1111/j.1365-246X.2004.02308.x
34. Kenyon, L.M., Wada, I.: Mantle wedge seismic anisotropy and shear wave splitting: effects of oblique subduction. J. Geophys. Res., Solid Earth **127**, 1–18 (2022). https://doi.org/10.1029/2021JB022752
35. Kenyon, L.M., Wada, I.: Shear-wave splitting in the mantle wedge: role of elastic tensor symmetry of olivine aggregates. Geophys. Res. Lett. **49**, 1–10 (2022). https://doi.org/10.1029/2022GL100143
36. Lev, E., Hager, B.H.: Prediction of anisotropy from flow models: a comparison of three methods. Geochem. Geophys. Geosyst. **9**(7), Q07014 (2008). https://doi.org/10.1029/2008GC002032
37. Lisbôa, T.V., Marczak, R.J.: Adomian decomposition method applied to anisotropic thick plates in bending. Eur. J. Mech. A, Solids **70**, 95–114 (2018). https://doi.org/10.1016/j.euromechsol.2018.02.002
38. Lisboa, T.V., Marczak, R.J., Bodmann, B.E.J., Vilhena, M.T.M.B.: Anisotropic fundamental solutions for linear elasticity and heat conduction problems based on a crystalline class hierarchy governed decomposition method. In: Constanda, C., Kirsch, A. (eds.) Integral Methods in Science and Engineering, pp. 361–373. Springer, Berlin (2015). https://doi.org/10.1007/978-3-319-16727-5_31
39. Löberich, E., Long, M.D., Wagner, L.S., Qorbani, E., Bokelmann, G.: Constraints on olivine deformation from SKS shear-wave splitting beneath the southern Cascadia subduction zone back-arc. Geochem. Geophys. Geosyst. **22**, 1–25 (2021). https://doi.org/10.1029/2021GC010091
40. Long, M.D., Hager, B.H., de Hoop, M.V., van der Hilst, R.D.: Two-dimensional modelling of subduction zone anisotropy with application to southwestern Japan. Geophys. J. Int. **170**, 839–856 (2007). https://doi.org/10.1111/j.1365-246X.2007.03464.x
41. MacDougall, J.G., Jadamec, M.A., Fischer, K.M.: The zone of influence of the subducting slab in the asthenospheric mantle. J. Geophys. Res., Solid Earth **122**, 6599–6624 (2017). https://doi.org/10.1002/2017JB014445

42. Mainprice, D., Bachmann, F., Hielscher, R., Schaeben, H.: Descriptive tools for the analysis of texture projects with large datasets using MTEX: strength, symmetry and components. In: Faulkner, D.R., Mariani, E., Mecklenburgh, J. (eds.) Rock Deformation from Field, Experiments and Theory: A Volume in Honour of Ernie Rutter, Special Publications, vol. 409, pp. 251–271. Geol. Soc., London (2015). https://doi.org/10.1144/SP409.8
43. Moakher, M., Norris, A.N.: The closest elastic tensor of arbitrary symmetry to an elassticity tensor of lower symmetry. J. Elast. **85**, 215–263 (2006). https://doi.org/10.1007/s10659-006-9082-0
44. Mondal, P., Long, M.D.: A model space search approach to finite-frequency SKS splitting intensity tomography in a reduced parameter space. Geophys. J. Int. **217**, 238–256 (2019). https://doi.org/10.1093/gji/ggz016
45. Morishige, M., Honda, S.: Three-dimensional structure of P-wave anisotropy in the presence of small-scale convection in the mantle wedge. Geochem. Geophys. Geosyst. **12**(12), Q12010 (2011). https://doi.org/10.1029/2011GC003866
46. Nippress, S.E.J., Kusznir, N.J., Kendall, J.M.: LPO predicted seismic anisotropy beneath a simple model of a mid-ocean ridge. Geophys. Res. Lett. **34**, L14309 (2007). https://doi.org/10.1029/2006GL029040
47. Norris, A.N.: Euler-Rodrigues and Cayley formulae for rotation of elasticity tensors. Math. Mech. Solids **13**, 465–498 (2008). https://doi.org/10.1177/1081286507077982
48. O'Driscoll, L.J., Humphreys, E.D., Schmandt, B.: Time corrections to teleseismic P delays derived from SKS splitting parameters and implications for western U.S. P-wave tomography. Geophys. Res. Lett. **38**, L19304 (2011). https://doi.org/10.1029/2011GL049031
49. Okaya, D., Vel, S.S., Song, W.J., Johnson, S.E.: Modification of crustal seismic anisotropy by geological structures ("structural geometric anisotropy"). Geosphere **15**(1), 146–170 (2019). https://doi.org/10.1130/GES01655.1
50. Satsukawa, T., Ildefonse, B., Mainprice, D., Morales, L.F.G., Michibayashi, K., Barou, F.: A database of plagioclase crystal preferred orientations (CPO) and microstructures – implications for CPO origin, strength, symmetry and seismic anisotropy in gabbroic rocks. Solid Earth **4**, 511–542 (2013). https://doi.org/10.5194/se-4-511-2013
51. Schulte-Pelkum, V., Mahan, K.: A method for mapping crustal deformation and anisotropy with receiver functions and first results from USArray. Earth Planet. Sci. Lett. **402**, 221–233 (2014). https://doi.org/10.1016/j.epsl.2014.01.050
52. Stanciu, A.C., Humphreys, E.D.: Seismic architecture of the upper mantle underlying California and Nevada. J. Geophys. Res., Solid Earth **126**, 1–21 (2021). https://doi.org/10.1029/2021JB021880
53. Tape, W., Tape, C.: Elastic symmetry with beachball pictures. Geophys. J. Int. **227**, 970–1003 (2021). https://doi.org/10.1093/gji/ggab183
54. Tape, W., Tape, C.: Two complementary methods of inferring elastic symmetry. J. Elast. **150**, 91–118 (2022). https://doi.org/10.1007/s10659-022-09898-0
55. VanderBeek, B.P., Faccenda, M.: Imaging upper mantle anisotropy with teleseismic P-wave delays: insights from tomographic reconstructions of subduction simulations. Geophys. J. Int. **225**, 2097–2119 (2021). https://doi.org/10.1093/gji/ggab081
56. VanderBeek, B.P., Lo Bue, R., Rappisi, F., Faccenda, M.: Imaging upper mantle anisotropy with traveltime and splitting intensity observations from teleseismic shear waves: insights from tomographic reconstructions of subduction simulations. Geophys. J. Int. **235**, 2640–2670 (2023). https://doi.org/10.1093/gji/ggad389
57. Walker, A.M., Wookey, J.: MSAT–a new toolkit for the analysis of elastic and seismic anisotropy. Comput. Geosci. **49**, 81–90 (2012). https://doi.org/10.1016/j.cageo.2012.05.031. https://github.com/andreww/MSAT/blob/master/msat/MS_axes.m
58. Walker, A.M., Wookey, J.: MSAT–a new toolkit for the analysis of elastic and seismic anisotropy. Comput. Geosci. **49**, 81–90 (2012). https://doi.org/10.1016/j.cageo.2012.05.031. https://github.com/andreww/MSAT/blob/master/msat/MS_decomp.m
59. Walker, A.M., Wookey, J.: MSAT–a new toolkit for the analysis of elastic and seismic anisotropy. Comput. Geosci. **49**, 81–90 (2012). https://doi.org/10.1016/j.cageo.2012.05.031. https://github.com/andreww/MSAT/blob/master/msat/MS_norms.m
60. Walker, A.M., Wookey, J.: MSAT–a new toolkit for the analysis of elastic and seismic anisotropy. Comput. Geosci. **49**, 81–90 (2012). https://doi.org/10.1016/j.cageo.2012.05.031. https://github.com/andreww/MSAT
61. Walker, A.M., Forte, A.M., Wookey, J., Nowacki, A., Kendall, J.M.: Elastic anisotropy of D″ predicted from global models of mantle flow. Geochem. Geophys. Geosyst. **12**(10), Q10006 (2011). https://doi.org/10.1029/2011GC003732
62. Ward, D., Mahan, K., Schulte-Pelkum, V.: Roles of quartz and mica in seismic anisotropy of mylonites. Geophys. J. Int. **190**, 1123–1134 (2012). https://doi.org/10.1111/j.1365-246X.2012.05528.x

63. Wolf, J., Long, M.D., Leng, K., Nissen-Meyer, T.: Sensitivity of SK(K)S and ScS phases to heterogeneous anisotropy in the lowermost mantle from global wavefield simulations. Geophys. J. Int. **228**, 366–386 (2022). https://doi.org/10.1093/gji/ggab347
64. Zaicenco, A.: Elasticity matrix inversion from VSP using orthogonal projectors. SEG Expanded Abstracts, 5082–5086 (2013). https://doi.org/10.1190/segam2013-0833.1